Error Estimation and Adaptive Mesh Refinement for Parallel Analysis of Shell Structures

SCOTT C. KEATING
CARLOS A. FELIPPA
K. C. PARK

Department of Aerospace Engineering Sciences and
Center for Aerospace Structures
University of Colorado
Boulder, Colorado 80309-0429, USA

November 1994

Report No. CU-CAS-94-23

Research supported by NASA Langley Research Center under Grant NAS1-756, monitored by Dr. J. Housner.

ERROR ESTIMATION AND ADAPTIVE MESH REFINEMENT FOR PARALLEL ANALYSIS OF SHELL STRUCTURES

SCOTT C. KEATING
CARLOS A. FELIPPA
K. C. PARK

Department of Aerospace Engineering Sciences
and Center for Aerospace Structures
University of Colorado, Campus Box 429
Boulder, CO 80309-0429, USA

ABSTRACT

We investigate the formulation and application of element-level, element-independent error indicators. Our research culminates in the development of an error indicator formulation which is derived based on the projection of element deformation onto the intrinsic element displacement modes. The qualifier 'element-level' means that no information from adjacent elements is used for error estimation. This property is ideally suited for obtaining error values and driving adaptive mesh refinements on parallel computers where access to neighboring elements residing on different processors may incur significant overhead. In addition such estimators are insensitive to the presence of physical interfaces and junctures. An error indicator qualifies as 'element-independent' when only *visible* quantities such as element stiffness and nodal displacements are used to quantify error. Error evaluation at the element level and element independence for the error indicator are highly desired properties for computing error in production-level finite element codes. Four element-level error indicators have been constructed. Two of the indicators are based on variational formulation of the element stiffness and are element-dependent. Their derivations are retained for developmental purposes. The second two indicators mimick and exceed the first two in performance but require no special formulation of the element stiffness and are therefore element-independent. We describe an algorithm for element-splitting mesh refinement which we demonstrate for two dimensional plane stress problems. We discuss the parallelizing of substructures and adaptive mesh refinement. We demonstrate the final error indicator using two-dimensional plane-stress and three-dimensional shell problems.

1. Introduction

Automated solution techniques for the finite element method are being implemented more and more frequently in the engineering sciences. As structures and structural models become increasingly complex, the need arises for techniques which require less interaction with the user while still returning accurate results. One particular advance in computational techniques is the use of parallel processing for both solution procedures and adaptive mesh refinement. High speed, multi-processor computers can return solutions in a fraction of the time needed by serial computers.

An important issue in adaptive mesh refinement is to establish the quality of the solution obtained in terms of discretization error. Many users of finite element analysis rely on convergence arguments to determine the accuracy or acceptability of a solution. In principle, meshes are refined until a convergent solution is obtained and that solution is generally accepted as correct. Another common procedure has been to quantify stress jumps between adjacent elements as a way to ascertain the quality of a displacement-based solution. These two approaches have obvious physical appeal to engineers.

Quantifying discretization error is usually performed using *a posteriori* error indicators. An indicator is said to be *element-independent* if the method for computing an error value relies only on *visible* or *derived* quantities readily obtained from the element. For displacement-based finite elements, these quantities consist of stiffness, displacement, stresses, or strains. Element-independence is paramount in establishing error estimations for existing finite element codes in which element formulations may be considered *black box* computations. The present research has evolved from element-dependent error estimation to error analysis more suited to production-level codes.

Error indicators are said to be *element-level* if they can be calculated without information from adjacent elements. This property is highly desirable in *massively parallel computations* in which individual elements or element groups are stored on different processing units. Element-level estimation reduces processor communication overhead, especially if neighboring elements are not stored on neighboring processors.

Another important issue in adaptive mesh refinement is the choice of methods by which to refine the mesh (or parts of the mesh). Principally, there are four techniques by which to refine meshes: node relocation – r-adaptation; element splitting – h-adaptation; element rezoning – z-adaptation; and modification of the element polynomial order – p-adaptation. Consideration of the p-adaptation technique will be ommitted from this research as it requires tremendous changes in data structures and is therefore unsuitable for efficient parallel analysis. Two of the remaining three techniques have been implemented in previous research and we offer justification for the implementation of the third in the sequel.

Decomposition of the finite element model into substructures is also a parallelizable process. Element groups are considered independently on individual processors where a solution step is performed. The solutions from several processors are then assembled and solved (usually via iterative methods) to create a complete solution for the structural

model. Hence, both the solution and mesh refinement phases of a complete analysis can be done in parallel.

We defined three goals by which to guide the research:

Goal 1. Development of an element-level error indicator capable of locating regions of error for single- and multiple-domain finite element meshes. The error indicator should not be affected by "jumps" due to material or geometric interfaces.

Goal 2. Development of an element-independent error indicator which meets the objectives of Goal 1 and is capable of returning reasonable estimates for mesh discretization energy error.

Goal 3. Application of the indicator to solving realistic shell structure problems using parallel analysis.

We present the progression from element-dependent error indicators to element-independent indicators. In the progression, the four error indicators are denoted sequentially as ϵ_1, ϵ_2, ϵ_3 and ϵ_4. We demonstrate the utility of the two element-independent error indicators with regard to adaptive mesh refinement and assess their potential for measuring strain energy error.

2. Historical Background

The importance of developing reliable and economical finite element error estimates has been recognized by a large number of researchers since the late 1970s. Substantial progress in this direction has been made over the past decade. The following survey highlights key sources and advances in what is presently an active area of research.

2.1. Bounding the Energy Error.

The first attempt to establish *a posteriori* error bounds in problems of structural mechanics was made in the early 1960s by Fraeijs DeVeubeke[1,2]; follow up work may be found in the Memorial Volume.[3] DeVeubeke advocated solving the structural problem twice, once with conforming elements and once with equilibrium elements, to obtain lower and upper bounds Π_- and Π_+, respectively, to the actual potential energy Π. The difference

$$\Delta\Pi = \Pi_+ - \Pi_- \qquad (2.1.1)$$

may serve as an overall indicator of discretization error because $\Delta\Pi \to 0$ as both meshes are refined. Bounds on pointwise errors can be derived through application of dummy forces and displacements and Castigliano's theorem. Each such estimation requires, however, the complete solution of two linear problems. Despite its elegance, this approach did not attract attention from finite element developers and users. Its key drawbacks are:

1. Two meshes have to be constructed. Because conforming and equilibrium elements have very different freedom configuration the two meshes do not have the same connectivity.

2. Equilibrium elements have never become popular because they are difficult to construct as well as expensive in terms of degrees of freedom and connectivity when used within a stiffness-based program. Similarly, purely conforming, exactly integrated elements are rarely used because they are too stiff.
3. The computation of local error estimators, which are needed to drive mesh refinement, is cumbersome and expensive. Even if they had been economical to obtain, adaptation would involve *simultaneously adapting two separate finite element models* while satisfying locality constraints. This leads to significant implementation difficulties.

2.2. Potential Energy Estimators.

A second idea emerged in the early 1970: node relocation based on energy minimization. Consider a mesh of *conforming* finite elements with visible degrees of freedom collected in vector $\mathbf{v}$. The potential energy

$$\Pi(\mathbf{v}) = U(\mathbf{v}) - W(\mathbf{v}) = \tfrac{1}{2}\mathbf{v}^T\mathbf{K}\mathbf{v} - \mathbf{p}^T\mathbf{v}, \tag{2.2.1}$$

is considered also a function of the *node locations:* $\Pi(\mathbf{v},\mathbf{x})$. In the linear case, $\Pi = \frac{1}{2}\mathbf{v}^T\mathbf{K}(\mathbf{x})\mathbf{v} - \mathbf{p}^T(\mathbf{x})\mathbf{v}$. For fixed $\mathbf{x}$, the solution $\mathbf{v} = \mathbf{K}^{-1}\mathbf{p}$ gives $\Pi(\mathbf{x}) = \mathbf{p}(\mathbf{x})\mathbf{K}(\mathbf{x})^{-1}\mathbf{p}(\mathbf{x})$. This can be minimized with respect to $\mathbf{x}$ to get an "optimal mesh" with the given topology and freedom configuration. This approach is now called r-adaptive mesh refinement, or the r-adaptation for short.

2.3. Local Estimators.

The idea leading to the selfadaptive h-method, or h-adaptation for short, was apparently first proposed in two papers by Babuška[4] and Sewell[5] that appeared on the same MAFELAP Proceedings volume. The article by Babuška was, however, more specifically oriented to applications and thus exerted bigger influence. These first error estimators for h-adaptation were of *residual* type. For the prediction phase many error indicators and error estimators have been developed over the past 15 years. The most successful ones are based on measuring discontinuities of derived field quantities such as stresses or strains across interelement boundaries. Other estimators are based on interpolating residual estimates considering element patches. In 1986 Zienkiewicz and Zhu[6] proposed an error estimator based on the smoothing of the stress jumps at element nodes. More recently, in 1992, Zienkiewicz and Zhu[7] proposed an improved error estimator with superconvergent characteristics. This has been widely adopted.

2.3.1. Zienkiewicz-Zhu Superconvergent Patch Recovery

We now briefly review the Zienkiewicz-Zhu (Z^2) superconvergent patch recovery for error estimation.[7] The basic measure used in Z^2 error estimation is an energy norm of the difference between a smoothed solution over an element patch and the derived values from the element. A patch is defined as a group of elements surrounding a node. In essence,

smoothing a solution over a patch effectively elevates the polynomial order by one. We confine our discussion to simple problems of linear hyperelasticity.

Define the smooth solution σ^* as

$$\sigma^* = \mathbf{P}\mathbf{a}. \tag{2.3.1}$$

where $\mathbf{P}$ is a polynomial basis representing the assumed displacement field of the element and $\mathbf{a}$ is a vector of unknown parameters. Minimizing the function

$$F(\mathbf{a}) = \sum_{i=1}^{n} \left(\sigma(x_i, y_i) - \mathbf{P}(x_i, y_i)\mathbf{a}\right)^2 \tag{2.3.2}$$

implies that

$$\mathbf{a} = \mathbf{A}^{-1}\mathbf{b} \tag{2.3.3}$$

where

$$\begin{aligned} \mathbf{A} &= \sum_{i=1}^{n} \mathbf{P}^T(x_i, y_i)\mathbf{P}(x_i, y_i), \\ \mathbf{b} &= \sum_{i=1}^{n} \mathbf{P}^T(x_i, y_i)\sigma(x_i, y_i). \end{aligned} \tag{2.3.4}$$

The number of sampling points, $n = mk$, is equal to the number m of elements surrounding a node times the number of sampling points k per element.

For two and higher dimenisonal problems, the Z^2 error estimate ϵ^{Z^2} on the element level is given as

$$||\epsilon^{Z^2}||_e = \int_{\Omega_e} (\boldsymbol{\sigma} - \boldsymbol{\sigma}^*)^T(\boldsymbol{\sigma} - \boldsymbol{\sigma}^*) d\Omega_e \tag{2.3.5}$$

where $\boldsymbol{\sigma}$ and $\boldsymbol{\sigma}^*$ are vectors of element-derived and smoothed stresses, respectively and Ω_e is the volume given of the element. Averaged nodal values used for error estimation are given by

$$||\epsilon^{Z^2}||_n = \left\{\sum_{i=1}^{N} \left(||\epsilon^{Z^2}||_e\right)^2\right\}^{\frac{1}{2}}. \tag{2.3.6}$$

By now there is a large and rapidly growing literature on FEM local error estimators. The surveys by Babuška[8], Zienkiewicz *et al.*[9,10,11,12] and the finite element book by Szabó and Babuška[13] may be recommended. In summary, it can be stated that present estimators work well for conforming elements, homogeneous domains and continuum-type linear problems. The reliance on jump conditions or the smoothing of the jumps brings difficulties, however, when such jumps are a natural part of the problem as in junctures, material interfaces, localization bands or shocks. Moreover, conforming elements are not necessarily the best performers in structural problems. We now investigate the development and application of four element-level error indicators.

3. Parameterized-Functional Error Indicators

Our original research of element-level error estimation is based on extraction of higher order element energy from high-performance elements. As described below, these elements are based on parameterized functionals and the development of two error indicators through specialized formulation has lead to Parameterized-Functional (PF) Error Estimation. While these particular error indicators require element-dependent formulation, their derivations have significant implications for the present research and are retained for developmental purposes.

3.1. Background

Felippa and Militello[14,15] introduced a general parametrized form of the stress-strain-displacement functional of linear hyperelasticity. A general expression for the functional is:

$$\Pi_{\alpha\beta\gamma} = U_{\alpha\beta\gamma} - P = U(\tilde{\mathbf{u}}, \tilde{\boldsymbol{\sigma}}, \tilde{\mathbf{e}}, \alpha, \beta, \gamma) - P, \tag{3.1.1}$$

where U is the generalized strain energy stored in the body volume, P is a forcing potential that embodies all other actions such as loading and boundary conditions, α, β and γ are free parameters further discussed below, and $\tilde{\mathbf{u}}$, $\tilde{\boldsymbol{\sigma}}$ and $\tilde{\mathbf{e}}$ are the varied displacements, stress, and strain fields, respectively. (A superposed tilde expresses that the symbol is subject to independent variation.) The variation $\delta\Pi = 0$ generates all governing equations of elasticity for arbitrary α, β and γ. All elasticity functionals with varied displacements can be obtained by appropriate specialization of these parameters.

As to the forcing potential P, three forms labelled as P^c, P^d and P^t have been studied in conjunction with parametrized functionals.[16,17,18,19,20] P^c is the conventional forcing potential, which is used in non-hybrid finite element discretizations. Potentials P^d and P^t, called displacement-generalized and traction-generalized, respectively, are useful in the construction of high-performance hybrid elements with additional boundary fields. Of these the displacement-generalized potential P^d has proven to be the most useful one in the construction of high-performance elements.[21] This potential depends on three varied fields

$$P^d = P^d(\tilde{\mathbf{u}}, \tilde{\boldsymbol{\sigma}}, \tilde{\mathbf{d}}), \tag{3.1.2}$$

where $\tilde{\mathbf{d}}$ is a boundary displacement field defined only at element interfaces. A common property of P^c, P^d and P^t is that they do not directly depend on the free parameters.

Now suppose that (3.1.1) is used to construct a finite element discretization, while keeping one or more parameters free. (Practically this means that such parameters are kept as arguments of the element stiffness subroutines.) The discrete approximants $\tilde{\mathbf{u}}$, $\tilde{\boldsymbol{\sigma}}$ and $\tilde{\mathbf{e}}$ obtained for a given mesh will then be generally functions of the free parameter(s). An important property of (3.1.1) is that U takes the *same* value if the varied fields $\tilde{\mathbf{u}}$, $\tilde{\boldsymbol{\sigma}}$, $\tilde{\mathbf{e}}$ are set to the exact solution fields $\mathbf{u}$, $\boldsymbol{\sigma}$, $\boldsymbol{\epsilon}$, independently of α, β and γ. Hence, we may expect that the difference between two values of U obtained for two different sets of parameters may provide a indicator on how far we are from the converged solution.

That is, the difference may be adopted as an error indicator. The most interesting feature of this indicator is that it naturally provides an *element-level* indicator, as the following development shows.

To tackle the general case first, suppose that the two sets of parameters are (α_1, β_1, γ_1) and (α_0, β_0, γ_0). The corresponding approximate values for displacements, strains and stresses obtained with a given mesh are ($\tilde{\mathbf{u}}_1$, $\tilde{\boldsymbol{\sigma}}_1$, $\tilde{\mathbf{e}}_1$) and ($\tilde{\mathbf{u}}_0$, $\tilde{\boldsymbol{\sigma}}_0$, $\tilde{\mathbf{e}}_0$), respectively. Denote by $U_1^e = U^e(\tilde{\mathbf{u}}_1, \tilde{\boldsymbol{\sigma}}_1, \tilde{\mathbf{e}}_1, \alpha_1, \beta_1, \gamma_1)$ and $U_0^e = U^e(\tilde{\mathbf{u}}_0, \tilde{\boldsymbol{\sigma}}_0, \tilde{\mathbf{e}}_0, \alpha_0, \beta_0, \gamma_0)$ the value of the generalized strain energy evaluated over the e^{th} element of that mesh. Then the PF element error indicator is defined as the difference

$$\epsilon_1^e = |U_1^e - U_0^e|, \tag{3.1.3}$$

where p denotes a parameterized-functional error indicator. This definition apparently requires that the problem be solved twice for a given mesh. It will be seen, however, that consideration of the structure of the stiffness matrices and their dependence on the free parameters allows the use of only one solution.

Let $\mathbf{K}^e$ be the stiffness matrix of an ANDES[22] element. This is a variant of the Assumed Natural Strain (ANS) formulation, a name coined by Park and Stanley.[23] Let $\mathbf{v}^e$ be the visible element degrees of freedom (those degrees of freedom in common with other elements, also called the *connectors*) and $\mathbf{p}$ the corresponding element node forces. Then the element stiffness equations decompose as

$$\mathbf{K}^e\mathbf{v}^e = (\mathbf{K}_b^e + \mathbf{K}_h^e)\,\mathbf{v}^e = \mathbf{p}^e. \tag{3.1.4}$$

$\mathbf{K}_b^e$ and $\mathbf{K}_h^e$ are called the *basic* and *higher order* stiffness matrices, respectively. The basic stiffness matrix, which is usually rank deficient, is constructed for *consistency*. The higher order stiffness matrix is constructed for *stability* and (in more recent work) *accuracy*. A decomposition of this nature, which also holds at the assembly level, was first obtained by Bergan and Nygård[24] in their derivation of the Free Formulation.

3.2. The First PF Error Indicator

With a view towards reducing the need for two solutions, the first PF indicator, PF1, is chosen as the difference between the element internal energies for $\alpha_1 = \alpha$ and α_0:

$$\begin{aligned}\epsilon_1^e &= |U_\alpha - U_{\alpha=0}| \\ &= \tfrac{1}{2}\int_V \left| \begin{Bmatrix} \tilde{\boldsymbol{\sigma}} \\ \boldsymbol{\sigma}^e \\ \boldsymbol{\sigma}^u \end{Bmatrix}_\alpha^T \mathbf{J}_\alpha \begin{Bmatrix} \mathbf{e}^\sigma \\ \tilde{\mathbf{e}} \\ \mathbf{e}^u \end{Bmatrix}_\alpha - \begin{Bmatrix} \tilde{\boldsymbol{\sigma}} \\ \boldsymbol{\sigma}^e \\ \boldsymbol{\sigma}^u \end{Bmatrix}_0^T \mathbf{J}_0 \begin{Bmatrix} \mathbf{e}^\sigma \\ \tilde{\mathbf{e}} \\ \mathbf{e}^u \end{Bmatrix}_0 \right| dV.\end{aligned} \tag{3.2.1}$$

Next we assume, without proof, that for two different parametrizations and for a 'good' mesh the following property holds: $\tilde{\boldsymbol{\sigma}}_\alpha \simeq \tilde{\boldsymbol{\sigma}}_0$, $\tilde{\mathbf{u}}_\alpha \simeq \tilde{\mathbf{u}}_0$, and $\tilde{\mathbf{e}}_\alpha \simeq \tilde{\mathbf{e}}_0$; but that $\tilde{\mathbf{e}}_\alpha \neq \mathbf{e}_\alpha^\sigma \neq \mathbf{e}_\alpha^u$, $\tilde{\mathbf{e}}_0 \neq \mathbf{e}_0^\sigma \neq \mathbf{e}_0^u$. In other words, corresponding fields in two different parametrizations

converge toward each other faster than do different fields for each parametrization. If this assumption holds we can approximate the error indicator (3.2.1) as

$$\epsilon_1^e = \tfrac{1}{2}\alpha \int_V (\tilde{\boldsymbol{\sigma}} - \boldsymbol{\sigma}^e)_\alpha^T (\mathbf{e}^\sigma - \tilde{\mathbf{e}})_\alpha \, dV. \tag{3.2.2}$$

Through algebraic manipulations this expression can be transformed[21] to

$$\epsilon_1^e = \tfrac{1}{2}(\mathbf{v}_\alpha^e)^T \mathbf{K}_h^e \mathbf{v}_\alpha^e, \tag{3.2.3}$$

where $\mathbf{v}_\alpha^e$ denote the element degrees of freedom calculated for the α solution. Physically (3.2.3) is the *higher order energy* (HOE) absorbed by the element. Since for ANDES elements (as well as for FF elements) the higher order stiffness matrix $\mathbf{K}_h^e$ is always available in separate form, this indicator is readily calculated in an element by element manner.

It should be noticed that the PF1 error indicator is related to that heuristically proposed by Melosh and Marcal[27] in the context of the SED (Strain Energy Density) method.

3.2.1. Important Properties of the PF1 Error Indicator.

The error indicator inherits the properties of the higher order stiffness. By construction the higher order stiffness verifies

$$\mathbf{K}_h^e \mathbf{v}_b^e = \mathbf{0}, \tag{3.2.4}$$

where $\mathbf{v}_b$ are the nodal displacements associated with a rigid body motion or a constant strain state. Actually $\mathbf{v}_b$ expands the null space of $\mathbf{K}_h$. Any other $\mathbf{v}^e$ can be decomposed as $\mathbf{v}^e = \mathbf{v}_b^e + \mathbf{v}_h^e$, where $\mathbf{v}_b^e$ is the projection of $\mathbf{v}^e$ on the null space of $\mathbf{K}_h^e$.

From these considerations we conclude that (3.2.3) automatically "filters out" the contributions to the displacement field from rigid body motions and constant strain states. Thus, in problems whose analytical solution consists of uniform strain states the error indicator vanishes over each element, in accordance with the fact that *any* mesh should solve those cases exactly. This statement may be extended to cases solved by constant strain states that jump at material or geometric interfaces, if such interfaces are modeled exactly by the finite element mesh. Other error indicators in present use *do not* verify this property.

3.2.2. Performance of PF1

The PF1 indicator has been tested extensively in numerical and adaptive mesh refinement studies[28,29] and is capable of capturing regions containing high strain gradients. However, the error measured by PF1 does not converge to the true strain energy error and is element-formulation dependent. Thus the requirements of Goal 2 are not met. With a view towards constructing an estimator which will return the true energy error, we turn to the next PF error indicator, PF2.

3.3. The Second PF Error Indicator

As previously stated, the PF1 indicator has the ability to locate high strain gradients near junctures and singular points. The PF1 indicator is useful for error indication and adaptive mesh refinement in problems which exhibit these characteristics but fails to return an accurate measure of strain energy error. We now describe the second PF indicator, PF2. PF2 partially fufills the requirements of Goal 2 in that a true measure of the element strain energy error is returned for some displacement fields. While this indicator has remains undeveloped (primarily due to its inherent formulation dependency), its derivation and application in numerical experiments have lead to the most recent form of the element-independent error indicators.

3.3.1. Determining Error by Energy Balance.

In order to estimate the true energy error we need to know precisely how an element behaves in a particular strain field. We now examine behavior of the three node Extended Free Formulation (EFF) high-performance triangle element[30] in a pure bending field. To determine the energy error for an EFF element we begin by applying a known displacement mode (in this case, a pure bending field) to an element patch as shown in Fig. 1. The analytical strain energy for this element patch is

$$U_{an} = \tfrac{1}{2} \int_V \mathcal{U} dV \tag{3.3.1}$$

where $\mathcal{U}$ is the strain energy density for the given displacement field. Strain energy for the finite element patch is given as usual by

$$U_{fe} = \tfrac{1}{2} \mathbf{v}^{eT} \mathbf{K}^e \mathbf{v}^e. \tag{3.3.2}$$

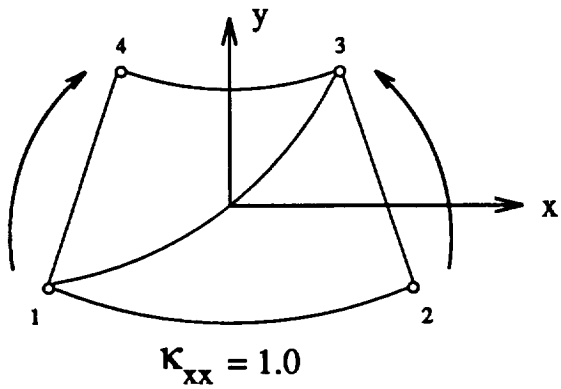

Fig. 1. Element patch of two EFF membrane triangle elements: Pure bending field.

The true strain energy error is defined as the difference between the analytical and finite element patch strain energies

$$\epsilon_{tr} = |U_{an} - U_{fe}|. \tag{3.3.3}$$

The element stiffness matrix $\mathbf{K}^e$ for the EFF triangle is decomposed as

$$\mathbf{K}^e = \mathbf{K}_b^e(\alpha_b) + \beta_b \mathbf{K}_h^e \tag{3.3.4}$$

where α_b is a variable scaling factor for the force-lumping scheme used in computing $\mathbf{K}_b$ and β_b is an overall scaling factor for $\mathbf{K}_h$. We wish to obtain a new stiffness matrix $\mathbf{K}'^e$ such that the element error is also given by

$$\epsilon_2^e = \tfrac{1}{2}(\mathbf{v}_h^e)^T \mathbf{K}'^e_h \mathbf{v}_h^e, \tag{3.3.5}$$

Symbolic solution for this element patch (setting $\epsilon_{tr}^e = \epsilon_2^e$) in pure bending yields two unknowns in two equations as coefficients for the element height H and height cubed H^3. From these equations we return a relationship from which α' and β' may be computed given α_b and β_b

$$\begin{aligned} \alpha' &= \frac{2\alpha_b - 3}{2} \\ \beta' &= \frac{5 - 4\alpha_b + 2\beta_b + 4\nu^2}{2}. \end{aligned} \tag{3.3.6}$$

The element strain energy error is then determined using (3.3.3).

3.3.2. Behavior of the PF2 Error Indicator

For the two-element patch in pure bending we are able to return a true measure of the strain energy error. However, numerical studies reveal that PF2 is highly sensitive to components of displacement modes other than pure bending. For example, Fig. 2 shows the effect of rotation of the third node beyond the pure bending field rotation. The rotation of node three is swept between ±10% of the pure bending rotation. Note that for Poisson's ratio $\nu = 0$, $\alpha_b = 3/2$ and $\beta_b = 1$, we obtain $\alpha' = 0$ (constant strain triangle stiffness) and $\beta' = 1/2$.

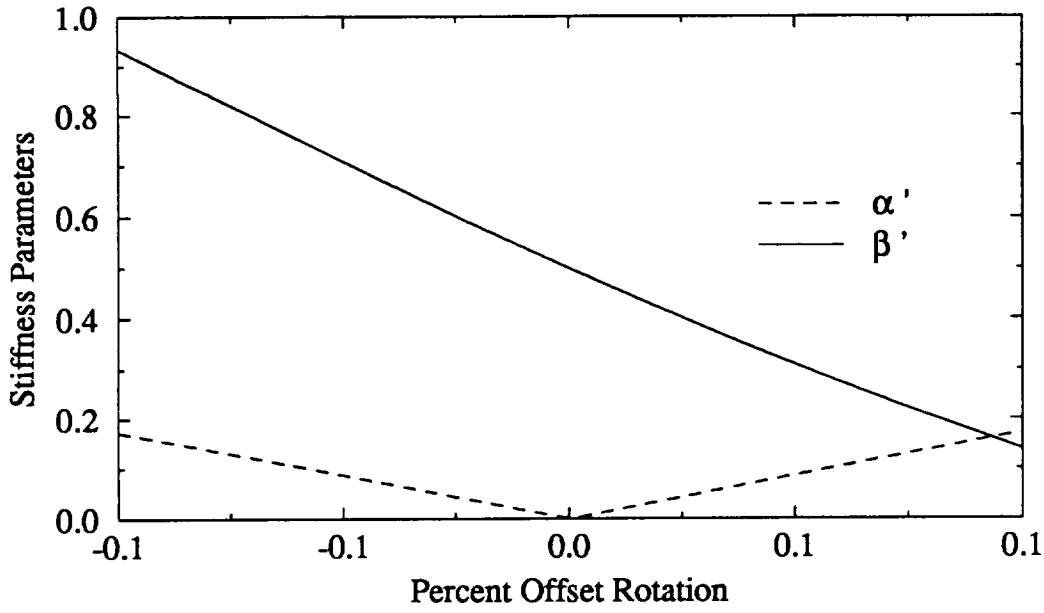

Fig. 2. Effect of Node 2 rotation beyond pure bending rotation: α' and β' values.

Clearly, the additional drilling rotation has a profound effect on the α' and β' values. Similar effects occur for other displacement modes applied to the element patch.

3.3.3. Toward an Element-Independent Error Indicator

From the PF1 and PF2 error indicators, we have established several important points regarding element behavior and error estimation:

1. All strain energy error is contained in the higher order element displacement modes. Therefore, filtering out basic (i.e., constant strain and rigid body) modes is desirable for computing an error measure. No contribution from basic modes also allows for error estimation despite "jump" conditions due to material and geometric discontinuities.
2. Error indicators are apparently sensitive to various displacement mode configurations of the element. This point requires us to quantify contributions to strain energy error from (higher order) modes experienced by the element.
3. High strain *gradients* are captured by both PF error indicators enabling these indicators to be used for structural problems in which analysis near singular points is desirable (e.g., linear-elastic fracture problems).

4. Element-Independent Error Indicators

The PF indicators provide an excellent base upon which to build error estimation ideas. The primary shortcomings of PF indicators and estimators are, of course, their element-formulation dependencies. In order to extend our error estimation ideas to *standard* finite elements, we introduce Element Independent (EI) error estimation. We have again constructed two error indicators in an attempt to mimick and then improve upon the PF indicators.

4.1. The EI Error Indicator

First, we wish to construct an EI error indicator that is capable of matching the performance of PF1 (i.e., one that will capture high strain gradients near junctures and singularities). Realization of this objective satisfies the element-level requirement stated in Goal 1. Development of this indicator, EI1, provides a step for our proceeding to meet the requirements in Goal 2.

4.1.1. Development of EI1

As previously shown, a property of the PF indicator is that strain energy due to lower strain modes is filtered out. This means that higher order strain energies are used to indicate element error. The question is then raised, "Can higher order strain energy from *any* finite element be used as an error indicator?" This is possible since *most* finite elements will produce higher strain modes, a method should be developed by which higher order energies for those elements could be extracted. With this thought in mind, we construct the EI1 indicator with characteristics similar to those of PF1.

Let us examine a decomposition of the total strain energy

$$U = \tfrac{1}{2}(\mathbf{v}^e)^T\mathbf{K}\mathbf{v}^e. \tag{4.1.1}$$

Splitting the displacement vector $\mathbf{v}$ into basic and higher order modes we can re-write the total strain energy as

$$\tfrac{1}{2}(\mathbf{v}^e)^T\mathbf{K}\mathbf{v}^e = \tfrac{1}{2}(\mathbf{v}_b^e)^T\mathbf{K}\mathbf{v}_b^e + (\mathbf{v}_b^e)^T\mathbf{K}\mathbf{v}_h^e + \tfrac{1}{2}(\mathbf{v}_h^e)^T\mathbf{K}\mathbf{v}_h^e. \tag{4.1.2}$$

The *basic* strain energy is

$$U_b = \tfrac{1}{2}(\mathbf{v}_b^e)^T\mathbf{K}\mathbf{v}_b^e. \tag{4.1.3}$$

Note that (4.1.2) is the energy equivalent of the total strain energy minus the HOE from the PF indicator. This is because $\mathbf{v}_b^e$ expands the null space of the higher order basis of $\mathbf{K}$. We define the *augmented* element HOE as

$$\begin{aligned} U_h^+ &= \tfrac{1}{2}(\mathbf{v}_h^e)^T\mathbf{K}\mathbf{v}_h^e \\ &= \tfrac{1}{2}(\mathbf{v}^e)^T\mathbf{K}\mathbf{v}^e - (\tfrac{1}{2}(\mathbf{v}_b^e)^T\mathbf{K}\mathbf{v}_b^e + (\mathbf{v}_b^e)^T\mathbf{K}\mathbf{v}_h^e) \end{aligned} \tag{4.1.4}$$

where the "+" indicates an additional energy term. The algebraic difference between U_h^+ and the previous HOE U_h (used as the PF1 indicator ϵ_1^e) is

$$U_h^+ - U_h = \tfrac{1}{2}(\mathbf{v}_h^e)^T(\mathbf{K}_b^e)^*\mathbf{v}_h^e \tag{4.1.5}$$

where $(\mathbf{K}_b^e)^*$ would be the ***basic*** element stiffness if such could be found.

Numerical experimentation shows that the term $\frac{1}{2}(\mathbf{v}_h^e)^T(\mathbf{K}_b^e)^*\mathbf{v}_h^e$ makes U_h^+ too *conservative* to be used for reasonable error indication. However, we can use U_h^+ as part of a scaling factor for the total strain energy to return *reasonable* values for error indication in regions of high strain gradients and in the vicinities of singularities.

We now define our EI1 indicator as

$$\begin{aligned}\epsilon_3^e &= \tfrac{1}{2}\,\frac{(\mathbf{v}_h^e)^T\mathbf{K}\mathbf{v}_h^e}{(\mathbf{v}_b^e)^T\mathbf{K}\mathbf{v}_b^e + (\mathbf{v}_h^e)^T\mathbf{K}\mathbf{v}_h^e}\,(\mathbf{v}^e)^T\mathbf{K}\mathbf{v}^e \\ &= \alpha_h U_{tot},\end{aligned} \tag{4.1.6}$$

where α_h is a scaling factor for the total strain energy U_{tot} and the superscript i indicates element-independence. Note that the element stiffness $\mathbf{K}$ remains intact for the error computation and requires no decomposition. In addition, the numerator of α_h in (4.1.6) contains only energies from higher order modes, meeting the requirement that "jump" conditions in constant strains will not affect the error measure.

The principal advantage of EI1 is that it can be used for error indication in standard finite elements, provided $\mathbf{v}_b$ and $\mathbf{v}_h$ are readily found. We now turn our attention toward decomposition of the displacement vector and computation of the necessary energy terms to construct EI1.

4.1.2. Obtaining Higher-Order Energy using Projectors

For simple planar elements (e.g., 3-node triangle), obtaining the higher order displacements $\mathbf{v}_h^e$ is relatively straightforward. To do this, we use a *projector* which filters out displacements for rigid body and constant strain modes. The projector, developed by Bjørn Haugen[31], is now defined. Recall the decomposition,

$$\mathbf{v}^e = \mathbf{v}_b^e + \mathbf{v}_h^e. \tag{4.1.7}$$

We write $\mathbf{v}_b^e$ as a linear combination of the rigid body and constant strain (basic) mode vectors

$$\mathbf{v}_b^e = \mathbf{R}\mathbf{a} \tag{4.1.8}$$

where $\mathbf{R}$ is a basis for $\mathbf{v}_b^e$ and $\mathbf{a}$ is a vector of coefficients such that

$$\mathbf{v}^e = \mathbf{R}\mathbf{a} + \mathbf{v}_h^e. \tag{4.1.9}$$

We require that the higher order displacement vector $\mathbf{v}_h^e$ be orthogonal to the basic modes such that

$$\mathbf{R}^T\mathbf{v}_h^e = \mathbf{0}. \tag{4.1.10}$$

Premultiplying $\mathbf{v}^e$ by the transpose of our basis matrix $\mathbf{R}$ and solving for $\mathbf{a}$ yields

$$\mathbf{a} = (\mathbf{R}^T\mathbf{R})^{-1}\mathbf{R}\mathbf{v}^e. \tag{4.1.11}$$

Upon rearrangement using (4.1.11) and (4.1.9) , we obtain

$$\begin{aligned} \mathbf{v}_h^e &= (\mathbf{I} - \mathbf{R}(\mathbf{R}^T\mathbf{R})^{-1}\mathbf{R}^T)\mathbf{v}^e \\ &= \mathbf{P}\mathbf{v}^e. \end{aligned} \tag{4.1.12}$$

Note that $\mathbf{P}^2 = \mathbf{P}$, which characterizes a projector matrix. The basic energy and augmented HOE are then computed using (4.1.3) and (4.1.4), respectively.

The projector algorithms for 3-node triangle elements have been implemented and tested to ensure that they extract the higher order displacement modes. They are now in use for computation of the EI1 indicator. Projectors for 3-node, 4-node and most planar elements are readily constructed with a second projector sometimes necessary, as in the case for *warped* 4-node elements. The projector method can also be extended to three-dimensional elements such as 8-node bricks. For more sophisticated elements with non-colinear nodes (e.g., doubly-curved shell elements), we will need other methods of determining error energy.

4.1.3. Obtaining Higher-Order Error Energy using Strain Averaging.

For higher order elements, the computation of error energy becomes somewhat more complex. In filtering out the basic modes by use of projectors, we are in effect subtracting an *average* strain energy from the total energy. To extend this concept to higher order elements, we write the basic energy in its integral form

$$U_b = \tfrac{1}{2}\int_V \bar{\boldsymbol{\sigma}}^T\bar{\mathbf{e}}dV. \tag{4.1.13}$$

and also write the augmented HOE in its integral form

$$U_h = \tfrac{1}{2}\int_V (\boldsymbol{\sigma} - \bar{\boldsymbol{\sigma}})^T(\mathbf{e} - \bar{\mathbf{e}})dV \tag{4.1.14}$$

where $\mathbf{e}$ and $\boldsymbol{\sigma}$ are the total strain and stress and $\bar{\mathbf{e}}$ and $\bar{\boldsymbol{\sigma}}$ are the averaged strain and stress, respectively. Define the *averaging* strain-displacement matrix as

$$\bar{\mathbf{B}} = \frac{1}{V}\int_V \mathbf{B}(\xi,\eta)dV \tag{4.1.15}$$

with

$$V = \int_V |\mathbf{J}(\xi,\eta)|d\xi d\eta \tag{4.1.16}$$

and ξ and η are the element natural coordinates and $\mathbf{J}(\xi,\eta)$ is the transformation Jacobian. The higher order strain and stress vectors are then

$$\begin{aligned} \mathbf{e}_h &= (\mathbf{e} - \bar{\mathbf{e}}) = (\mathbf{B} - \bar{\mathbf{B}})\mathbf{v}, \\ \boldsymbol{\sigma}_h &= (\boldsymbol{\sigma} - \bar{\boldsymbol{\sigma}}) = \mathbf{C}\mathbf{e}_h \end{aligned} \tag{4.1.17}$$

with $\mathbf{C}$ being the element constitutive matrix. Our EI error indicator is then defined as

$$\epsilon_3^e = \frac{U_h}{U_b + U_h} U_{tot}. \tag{4.1.18}$$

As presented, this method requires knowledge of the element strain-displacement matrix $\mathbf{B}$. This detracts somewhat from the idea of a truly element-independent error indicator. However, in lieu of using the actual $\mathbf{B}$ matrix, we may *assume* a strain-displacement relationship $\mathbf{B}^*$ provided we have *a priori* knowlege of the general element displacement capabilities. Our error indication may then be obtained by substituting $\mathbf{B}^*$ into (4.1.15) and (4.1.16) and computing ϵ_3^e using (4.1.18).

4.2. The Deformation Mode Error Indicator

We have seen from the development of the PF1, PF2 and EI1 indicators that strain energy error occurs in higher deformation modes and that the error indicators appear to be sensitive to *how much* of the higher modes experienced by the finite element. Therefore, we propose that quantifying the strain energy error necessitates determining *amounts* of error contained in the higher modes and the extent to which each of the modes is represented for a finite element in a given displacement field. We introduce a new error indicator based on projection of the element deformation onto the intrinsic element displacement modes which we call the Deformation Mode (DM) Error Indicator.

The DM error indicator offers promising results toward realizing both Goals 1 and 2. At present, DM has the capability of returning true energy errors in some displacement fields and a reasonable representation of error in others. We begin with the derivation of the indicator for planar two-dimenisonal elements and evaluate performance of the indicator with example problems in the sequel.

4.2.1. Derivation of the Deformation Mode Error Estimator.

A basis for the displacement modes of a finite element is given by the eigenvectors of the element stiffness matrix

$$\boldsymbol{\Psi} = \mathbf{eig}(\mathbf{K}). \tag{4.2.1}$$

An alternate basis is determined considering the known-mode displacements, which have a physical appeal with regard to *a priori* knowledge about continuum mechanics for those displacements. We define this second set of eigenvectors as

$$\boldsymbol{\Phi} = \mathbf{eig}(\mathbf{K}) \tag{4.2.2}$$

where $\boldsymbol{\lambda}$ such that

$$\mathbf{diag}(\boldsymbol{\lambda}) = \boldsymbol{\Phi}^T \mathbf{K} \boldsymbol{\Phi} \tag{4.2.3}$$

are the eigenvalues of $\mathbf{K}$ as usual.

For the present, we assume that the displacement field within an element domain is comprised of a linear combination of the known displacement modes of the finite element. Obviously, the finite element approximation to the displacement field is comprised of these modes.

The analytical strain energy for any of these modes is readily computed by integrating the strain energy density $\mathcal{U}_k$ for that mode over the element domain

$$U_{an}^k = \int_V \mathcal{U}_k dV, \tag{4.2.4}$$

where $k = 1, \ldots, n$ specifies which of the n modes is being considered. The strain energy for the finite element is

$$U_{fe}^k = \tfrac{1}{2} (\mathbf{v}^k)^T \mathbf{K} \mathbf{v}^k \tag{4.2.5}$$

and the strain energy error for the k^{th} mode is given as

$$m_k = U_{an}^k - U_{fe}^k. \tag{4.2.6}$$

Choosing an acceptable displacement field for the analytical field and requiring that the finite element match that field at the nodal points, we compute the error energy for the element in the prescribed mode using (4.2.4). We now have a *scalable* error value for the finite element in each of its modes. These error values are then collected into the modal error vector

$$\mathbf{m} = \begin{Bmatrix} m_1 \\ m_2 \\ \vdots \\ m_k \end{Bmatrix}. \tag{4.2.7}$$

We propose that the apparent energy error for the finite element is a superposition of the *amounts* of error contained within each of the displacement modes.

To determine the amount of error attributable to each mode, the finite element displacement vector is decomposed into its modal components using the inverse of the eigenvectors of the stiffness matrix

$$\boldsymbol{\alpha}_m = \boldsymbol{\Phi}^{-1} \mathbf{v}. \tag{4.2.8}$$

The modal component vector $\boldsymbol{\alpha}_m$ represents the magnitude of each of the modes seen in the element displacement field. The finite element strain energy is then written

$$U_{fe} = \boldsymbol{\alpha}_m^T \boldsymbol{\Phi}^T \mathbf{K} \boldsymbol{\Phi} \boldsymbol{\alpha}_m. \tag{4.2.9}$$

Recalling the assumption that the analytical displacement fields can be represented by the eigenvectors Φ of $\mathbf{K}$, and that the element nodal displacements can be decomposed into their respective modes, we have a means by which to compute an error measure for the element. Because the eigenvectors Φ diagonalize $\mathbf{K}$, we can write the error for the k^{th} mode as

$$\epsilon_4^k = \alpha_k^2 m_k. \tag{4.2.10}$$

The total DM error ϵ_4^e is then obtained by

$$\epsilon_4^e = \alpha_1^2 m_1 + \alpha_2^2 m_2 + \ldots + \alpha_n^2 m_n. \tag{4.2.11}$$

where α_i and m_i are the modal component and modal error vectors, respectively.

4.2.2. Application of DM to Shell Elements.

Obviously, some finite elements can represent displacement fields for which analytical complements are not easily found. This problem is resolved by "borrowing" surface modeling techniques from computer- aided design and manufacture (CAD and CAM).

Here, we define a 4-node element in parametric form using a tensor-product Ferguson surface patch (FSP).[32] The FSP is used as it relies on corner conditions which are derived readily from nodal values of the finite element. Fig. 3 shows a FSP with the corner conditions depicted in vector form (subscripts indicate derivative quatities and superscripts denote corner points).

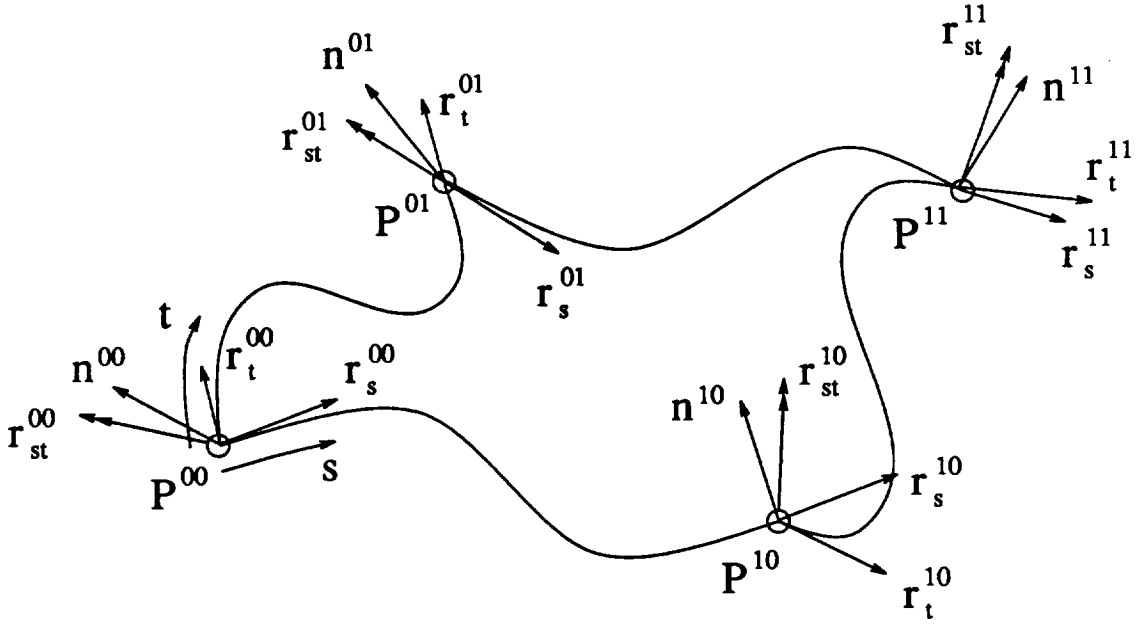

Fig. 3. Ferguson Surface Patch.

We define the FSP equation as

$$r_i(s,t) = \mathbf{SCQC}^T\mathbf{T}^T \tag{4.2.12}$$

where

$$\begin{aligned}
\mathbf{S} &= \begin{bmatrix} 1 & s & s^2 & s^3 \end{bmatrix} \qquad 0 \le s \le 1, \\
\mathbf{T} &= \begin{bmatrix} 1 & t & t^2 & t^3 \end{bmatrix} \qquad 0 \le t \le 1, \\
\mathbf{C} &= \begin{bmatrix} 1 & 0 & 0 & 0 \\ 0 & 0 & 1 & 0 \\ -3 & 3 & -2 & -1 \\ 2 & -2 & 1 & 1 \end{bmatrix}, \\
\mathbf{Q} &= \begin{bmatrix} P_{00} & P_{01} & \frac{\partial \mathbf{r}}{\partial t}|_{00} & \frac{\partial \mathbf{r}}{\partial t}|_{01} \\ P_{10} & P_{11} & \frac{\partial \mathbf{r}}{\partial t}|_{10} & \frac{\partial \mathbf{r}}{\partial t}|_{11} \\ \frac{\partial \mathbf{r}}{\partial s}|_{00} & \frac{\partial \mathbf{r}}{\partial s}|_{01} & \frac{\partial^2 \mathbf{r}}{\partial s \partial t}|_{00} & \frac{\partial^2 \mathbf{r}}{\partial s \partial t}|_{01} \\ \frac{\partial \mathbf{r}}{\partial s}|_{10} & \frac{\partial \mathbf{r}}{\partial s}|_{11} & \frac{\partial^2 \mathbf{r}}{\partial s \partial t}|_{10} & \frac{\partial^2 \mathbf{r}}{\partial s \partial t}|_{11} \end{bmatrix}.
\end{aligned} \tag{4.2.13}$$

Here, P and $\mathbf{r}$-derivatives denote the (x, y, z) coordinate triples and corner configurations for the FSP, respectively. Subscripts 00, 01, 10 and 11 specify the corner points for which each value is given.

The eigenvector modes of standard shell finite elements contain no information about the cross derivatives ("twists") at the node points which are necessary to complete the lower right 2×2 portion of $\mathbf{Q}$ in (4.2.13). To obtain a reasonable model for the finite element displacement modes, we need to estimate these twists somehow. As we wish to compute energy error for each of the finite element modes, we will use an energy-minimizing twist estimator based on a variational approach. A survey of other twist-estimation procedures is given by Farin.[33]

The functional

$$J = \int_\Omega (\kappa_{min}^2 + \kappa_{max}^2) d\Omega \tag{4.2.14}$$

is given by Nowacki, Reese[34] and Walter[35] as a fairness criterion for surfaces in engineering. The minimum and maximum normal section curvatures are κ_{min} and κ_{max}, respectively. This functional is used because it is a measure of the strain energy of flexure and torsion for a thin rectangular plate under small deflections. Hagen and Schulze have used this functional for twist estimation of patches with orthogonal boundary curves.[36] Farin has extended it to include nonorthogonal patch boundaries giving an estimate for the normal component of twist at a point as[37]

$$\mathbf{n}^T \frac{\partial^2 \mathbf{r}}{\partial s \partial t} = \frac{h}{g} \tag{4.2.15}$$

where

$$h = \frac{\partial \mathbf{r}^T}{\partial s}\frac{\partial \mathbf{r}}{\partial t}\left(\frac{\partial \mathbf{r}^T}{\partial s}\frac{\partial \mathbf{r}}{\partial s}\mathbf{n}^T\frac{\partial^2 \mathbf{r}}{\partial t^2} + \frac{\partial \mathbf{r}^T}{\partial t}\frac{\partial \mathbf{r}}{\partial t}\mathbf{n}^T\frac{\partial^2 \mathbf{r}}{\partial s^2}\right) \tag{4.2.16}$$

and

$$g = \frac{\partial \mathbf{r}^T}{\partial s}\frac{\partial \mathbf{r}}{\partial s}\frac{\partial \mathbf{r}^T}{\partial t}\frac{\partial \mathbf{r}}{\partial t} - (\frac{\partial \mathbf{r}^T}{\partial s}\frac{\partial \mathbf{r}}{\partial t})^2. \tag{4.2.17}$$

The tangential components of the twist vector are presumed small and set to zero.

From the preceeding formulation we construct element "surfaces" for the deformed and undeformed shapes of the element, $\mathbf{r}(s,t)$ and $\mathbf{r}^0(s,t)$, respectively. The deformation field $\mathbf{u}(s,t)$ is defined as

$$\mathbf{u}(s,t) = \mathbf{r}(s,t) - \mathbf{r}^0(s,t) \tag{4.2.18}$$

from which strains and strain energies can be derived. The analytical and finite element strain energies for a given mode are computed using (numerical integration of) (38) and (39), respectively.

4.2.3. Additional Energy Terms.

The true displacement field for a mesh region may of course contain displacements not represented by the displacement modes of the finite element. Including the strain energy from these displacements we rewrite (45) as

$$\epsilon_t = \alpha_1^2\epsilon_1 + \alpha_2^2\epsilon_2 + \ldots + \alpha_n^2\epsilon_n + \hat{U}_{an}, \tag{4.2.19}$$

where $\hat{U}_{an}$ is the strain energy not included in the finite element approximation. Assumedly, the additional strain energy $\hat{U}_{an}$ will come from higher order or cross-term displacement modes and may or may not decrease with mesh refinement.

5. Example Problems

We now demonstrate the applicability of the two element-independent error indicators. For the EI indicator we examine a simple linear elastic fracture problem and demonstrate the h-adaptation refinement. Additionally, we show the performance of the DM indicator in membrane- and bending-dominated problems. We will see that the EI indicator performs well for finding regions of high strain gradients and that the DM indicator qualitatively matches the Z^2 error estimator.

5.1. Example of EI1: An Application to h-adaptation Mesh Refinement.

We have shown how higher order energy can be extracted from a finite element to produce an indication of high strain gradients. We demonstrate the following h-adaptation algorithm in the context of a simple linear fracture problem given in the Example Problems section.

In previous work,[28,29] we describe and demonstrate the r-adaptive (node relocation) mesh refinement method. As an accompaniment to our research involving error indicators is used in element-splitting of three-node triangle elements.

Briefly, the logic used for h-adaptation is as follows:

1. Flag a percentage of the elements which exhibit the highest error for "splitting."
2. Inject nodes on the edges of the elements flagged for splitting. Assign surface parameters and boundary conditions to the new nodes.
3. Determine the number of new elements required and insert them accordingly. This is performed in passes to avoid creating "island" elements – unsplit elements surrounded by split elements – which create incompatibility.
4. Recompute error and follow-up with additional refinements as necessary to achieve a desired tolerance or convergence.

The h-adaptation method is essentially the division of single elements to multiple elements. This effect may prove useful in augmenting error measures as the solution converges.

Fig. 4 shows a standard linear-elastic fracture problem of a simply supported beam with a vertical crack. Figs. 5 and 6 show the original mesh and the meshes resulting from two h-adaptations. Mesh refinement occurs as expected near the cracktip, applied load and boundary conditions.

The EI1 error indicator performs well in determining the areas of high strain gradients for refinement. We conclude that while the EI1 indicator will not return proper strain energy error distribution, it can be successfully used in problems involving singularities.

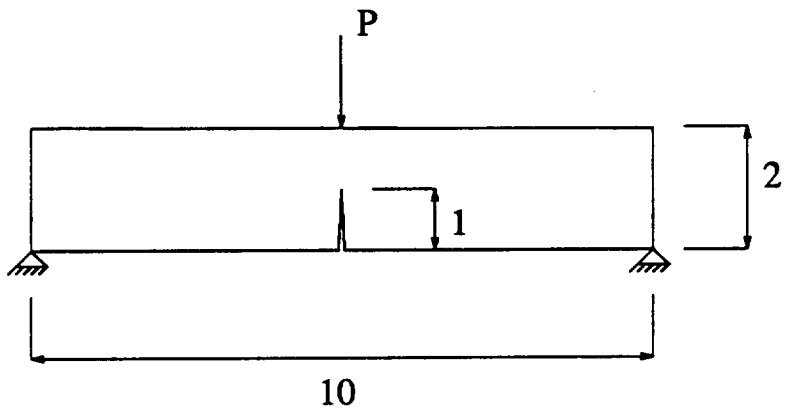

Fig. 4. Linear Elastic Fracture Problem.
Original mesh has 160 3-node triangle elements.

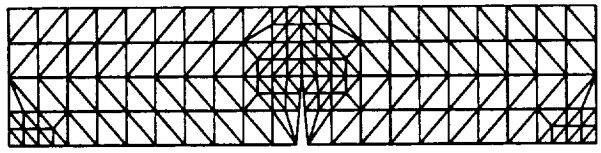

Fig. 5. Linear Elastic Fracture Problem.
Mesh after one h-adaptation.

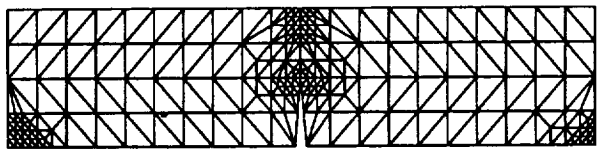

Fig. 6. Linear Elastic Fracture Problem.
Mesh after two h-adaptations.

5.2. Examples of DM Using 4-node Isoparametric Elements

We now demonstrate the DM indicator for three plane stress problems using four-node isoparametric plane stress quadrilateral elements. In lieu of deriving the higher order membrane displacement fields, via the FSP, we will assign pure bending fields (i.e., quadratic fields) based on the two higher mode eigenvectors for this element.

5.2.1. DM Error Indicator: Membrane Cantilever with Applied End Rotation

Our first problem used to assess the DM indicator is a membrane cantilever, built-in on one end with an applied rotation to the opposite end. Four meshes were used to model this problem. The applied rotation creates a constant curvature for the analytical solution. Fig. 7 shows one of the meshes (4×40 plane stress four-node quadrilateral elements) used to test DM in a pure bending field. Aspect of the cantilever is $10 : 1$.

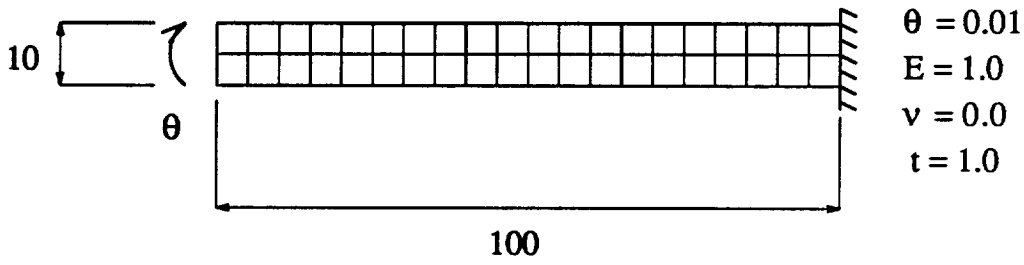

Fig. 7. Membrane Cantilever Problem (2×20) elements:
Built-in end with applied end rotation.
For all elements: $U_{fe} = 0.011719$, $U_{an} = 0.010417$,
$\epsilon_{an} = \epsilon_{fe} = 0.001302$.

DM returns the true strain energy error for each of the meshes tested (grids of 1×10, 2×20, 4×40, and 8×80 elements). These tests, and those conducted on single elements in the development of DM, verify the ability of DM to decompose the displacement field $\mathbf{v}$ into its componenent modes.

5.2.2. DM Error Indicator: Membrane Cantilever with Applied End Shear

Our second example for the DM indicator is a membrane cantilever, shown in Fig. 8. The analytical displacement solution is cubic leading to a quadratic strain field. We can assess

the effect of $\hat{U}$ of (40) on the error estimate as we uniformly refine the mesh as the strain energy due to shear is not modeled by the four node quad.

We start with a coarsely-meshed model with 10 elements. Fig. 9 shows that the DM indicator slightly overestimates the true error. Next we refine the mesh by halving the element size (40 elements). Now DM begins to underestimate the true error as shown in Fig. 10. The finite element strain energy is within about 12% near the root end and the computed free end tip displacement is about 90% of the analytical value.

Continuing to uniformly refine the mesh we see that the error indicator begins to greatly underestimate the analytical error. In Fig. 11 we see that the high energy errors near the outer edges of the cantilever at the root end are not captured by the DM indicator. Because of the uniform mesh refinement, the stiffness $\mathbf{K}^e$ for all elements is the same from mesh to mesh. Thus we conclude that indeed $\hat{U}$ of (40) exists and is comprised of strain energies not captured by the DM indicator.

However, it is also worth noting in the regions of apparently high error, that the true error has decreased to less than 4% of the total strain energy and that the tip displacement is 97% of the analytical value. DM also consistently predicts higher error (though underestimated) toward the root of the cantilever. This means that mesh refinement would still tend to refine the mesh in the regions of highest error.

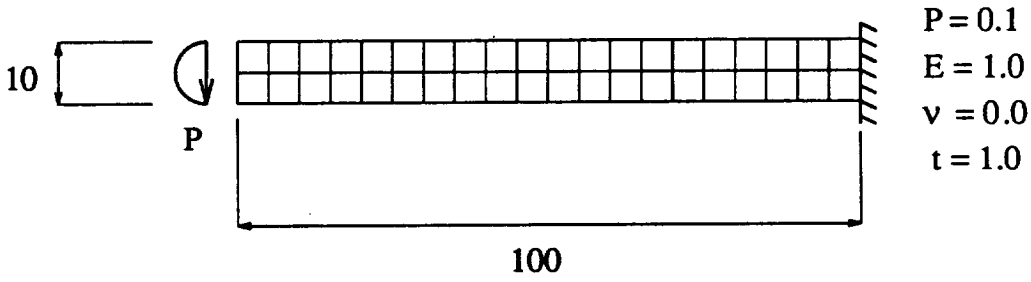

Fig. 8. Membrane Cantilever Problem:
Built-in end with applied end shear.

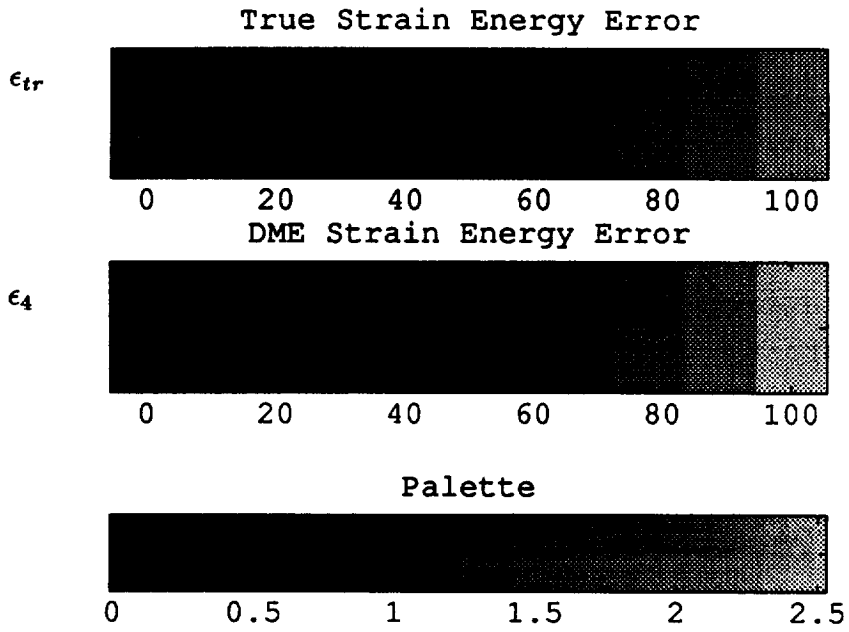

Fig. 9. Membrane cantilever with end shear, (1 x 10) elements: Comparison of true strain energy error to DM indicator error.

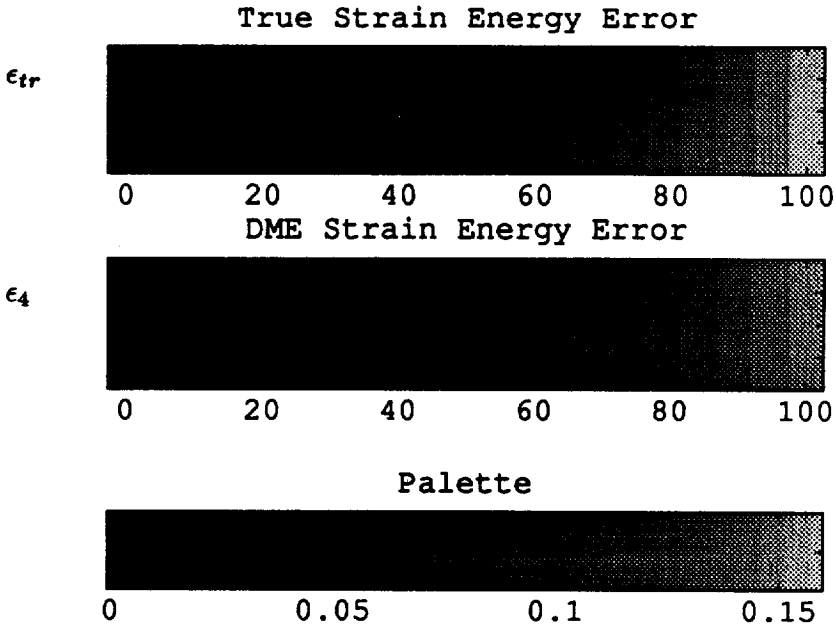

Fig. 10. Membrane cantilever with end shear, (2 x 20) elements: Comparison of true strain energy error to DM indicator error.

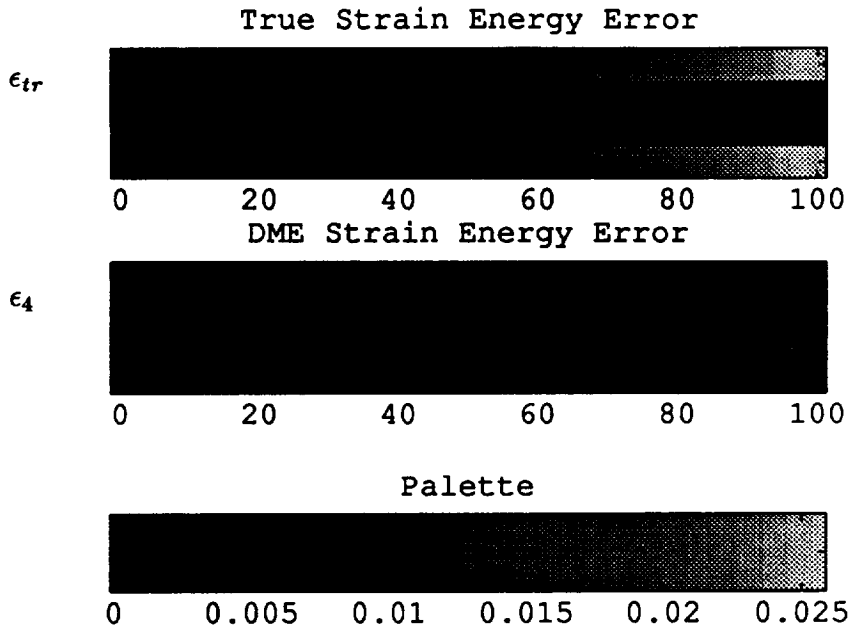

Fig. 11. Membrane cantilever with end shear, (4 x 40) elements: Comparison of true strain energy error to DM indicator error.

5.2.3. DM Error Indicator: Sharp Strain Gradients

We now observe the performance of the DM indicator for capturing high errors in regions of sharp strain gradients. This problem was proposed by Oden *et al.*[38] and used by Zienkiewicz and Zhu[7] for testing their error estimator.

The proposed problem is given as

$$u = x(1-x)y(1-y)\tan^{-1}(\alpha(\xi - \xi_0)) \tag{5.2.1}$$

with recommended values of

$$\begin{aligned} \xi &= \frac{(x+y)}{\sqrt{2}} \\ \xi_0 &= 0.8 \\ \alpha &= 20. \end{aligned} \tag{5.2.2}$$

The governing equation of the problem is

$$-\Delta u = f \tag{5.2.3}$$

with boundary conditions $u = 0$ on $\partial\Omega$ where Ω is a unit square domain on $(0,1) \times (0,1)$. Figs. 12(a) and 12(b) show the contours of $\partial u/\partial x$ and $\partial u/\partial y$, indicative of the strain gradients in x and y.

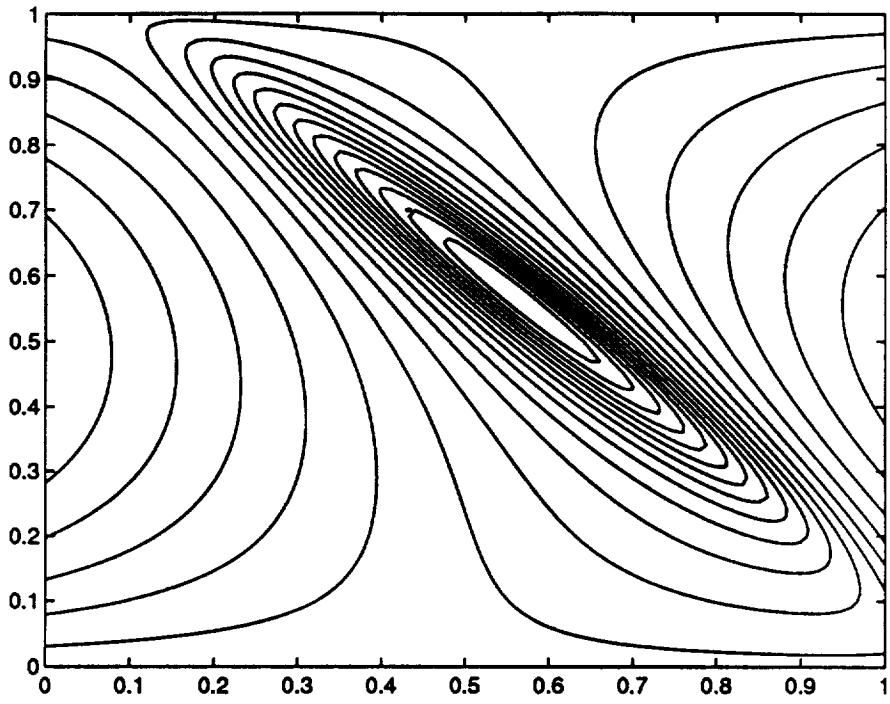

Fig. 12(a) Contour of $\partial u/\partial x$ for (5.2.1).

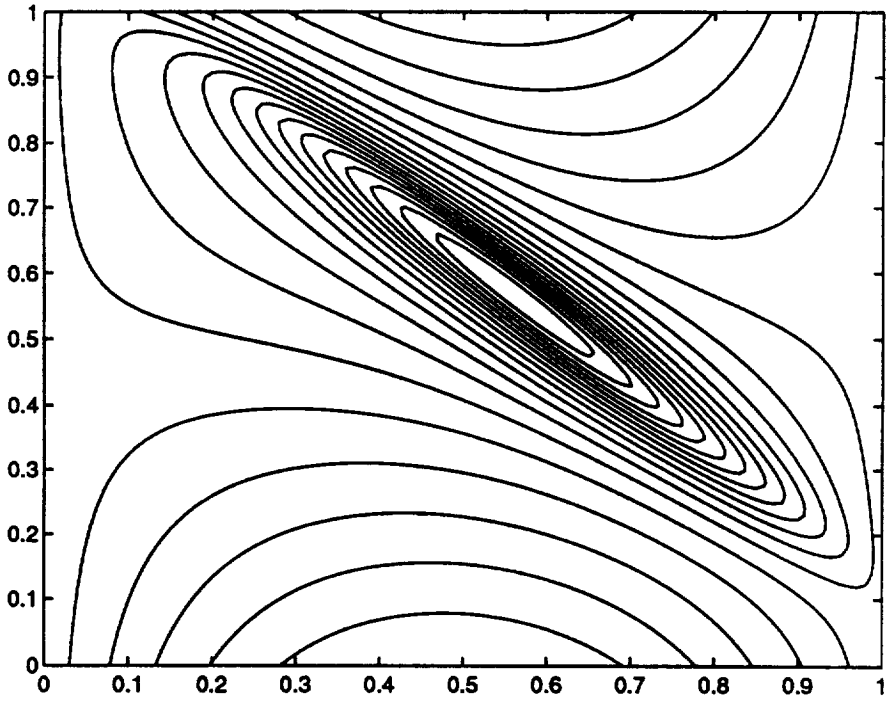

Fig. 12(b) Contour of $\partial u/\partial y$ for (5.2.1).

Figs. 13, 14 and 15 show the performance of the DM indicator with respect to capturing sharp strain gradients while uniformly refining the mesh: 5×5, 20×20, and 50×50 isoparametric quadrilateral elements, repectively. Referring to Fig. 12, we see that increased error is predicted in the regions accompanying the high gradient. Addtionally, visual comparison with the exact solution and patch-recovery error estimator of Zienkiewicz and Zhu[7] is favorable.

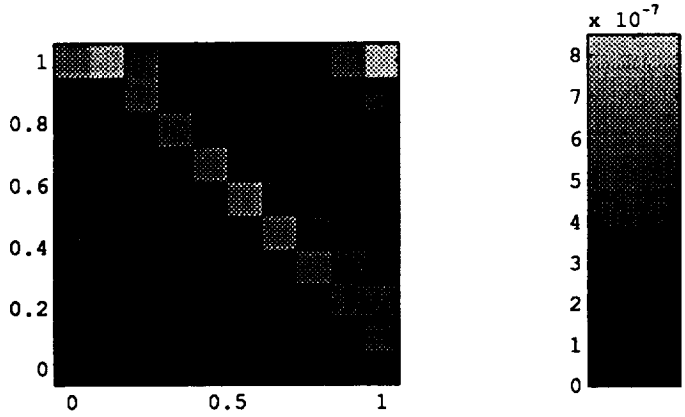

Fig. 13. Sharp strain gradients (Oden):
DM error indicator
(10 x 10) elements.

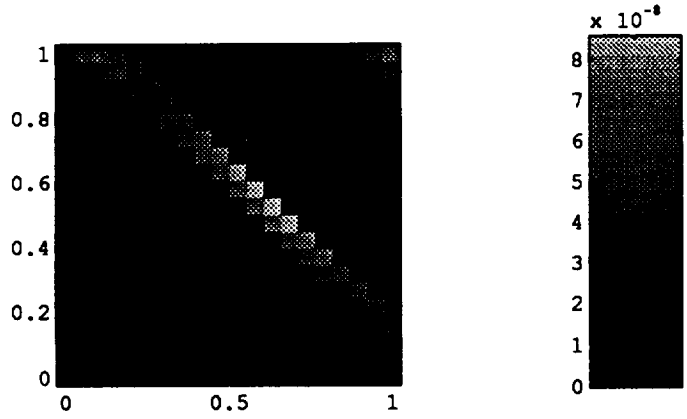

Fig. 14. Sharp strain gradients (Oden):
DM error indicator
(20 x 20) elements.

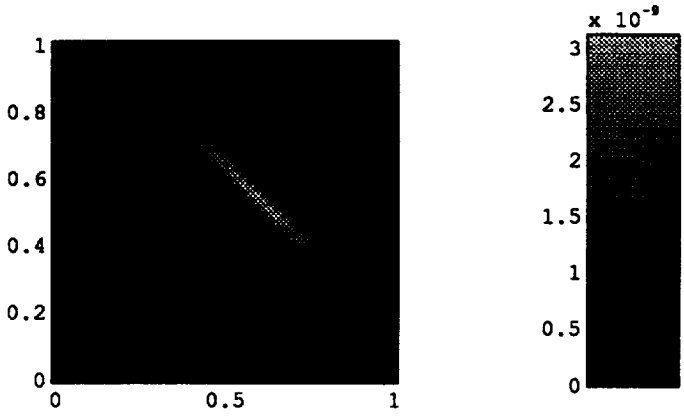

Fig. 15. Sharp strain gradients (Oden):
DM error indicator
(50 x 50) elements.

5.2.4. Example of DM Using 4-node ANS Shell Elements

We now demonstrate DM using the benchmark cylinder-plate juncture (CPJ) problem developed previous work.[29] Fig. 16 gives geometric, material, load and B.C. data for the CPJ problem. We compare our DM indicator with a refined model tested at the Structures Laboratory at Lockheed PARL.[39] All analyses of the CPJ problem are modeled using quarter symmetry.

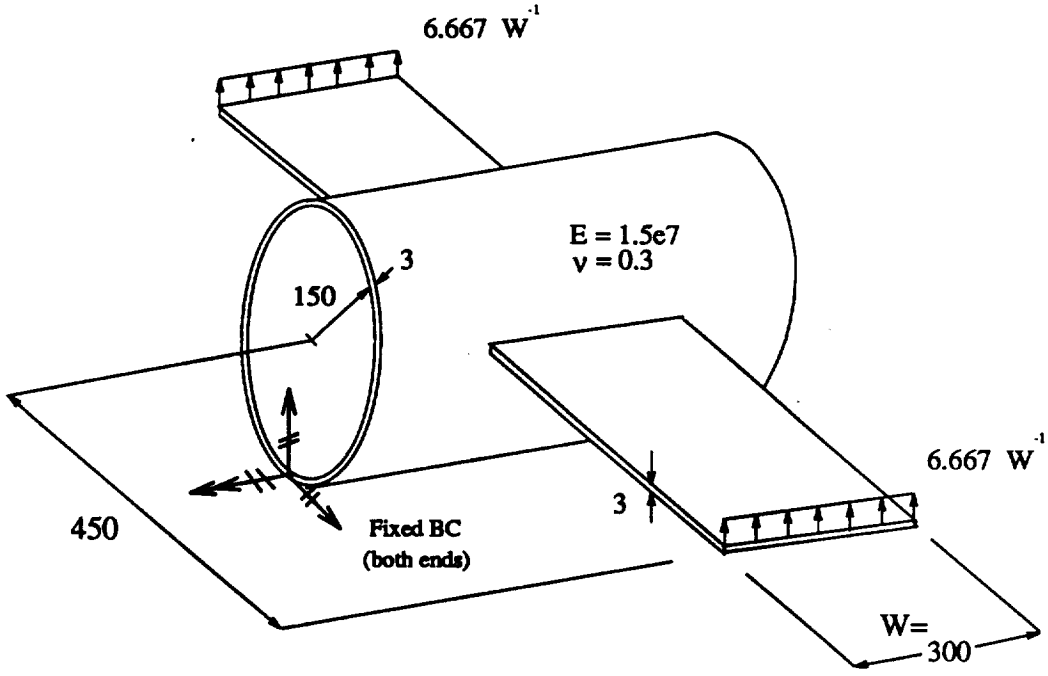

Fig. 16. Benchmark problem featuring cylinder-plate junctures.
The cylindrical shell is supported by end diaphrams, with
fixed derees of freedom as shown.

Plate 1 shows the relative error distribution determined by the Lockheed testbed code for a mesh of 320 16-node ANS shell elements. For all plates, the error ranges blue to red from low error to high error, respectively. The Lockheed solution is based upon the Zienkiewicz-Zhu[6] error estimator using special mesh partitioning to remove the effects of the juncture. Plates 2 and 3 show the performance of the DM indicator for meshes of 320 and 1056 4-node Assumed Natural Strain - Equilibrium Constrained (ANS-EC) elements.[40] The ANS-EC 4-node element belongs to the class of C^0 plate/shell elements. Higher-order contributions to the element stiffness are given from a strain-displacement matrix which is not derived from the standard Lagrange shape functions, but is instead derived from the imposition of kinematic and equilibrium constraints.

We see from Plates 2 and 3 that the DM indicator qualitatively matches the results from the Lockheed error estimation shown in Plate 1. The mesh in Plate 2 uses the same number of elements as used for the Lockheed model in Plate 1. Plate 3 shows a similar error distribution along the juncture. Note that in all cases, the error is primarily confined to the single rows of elements directly on either side of the CPJ. To date, the DM indicator for shell elements has not been tested quantitatively to establish its potential for true error estimation.

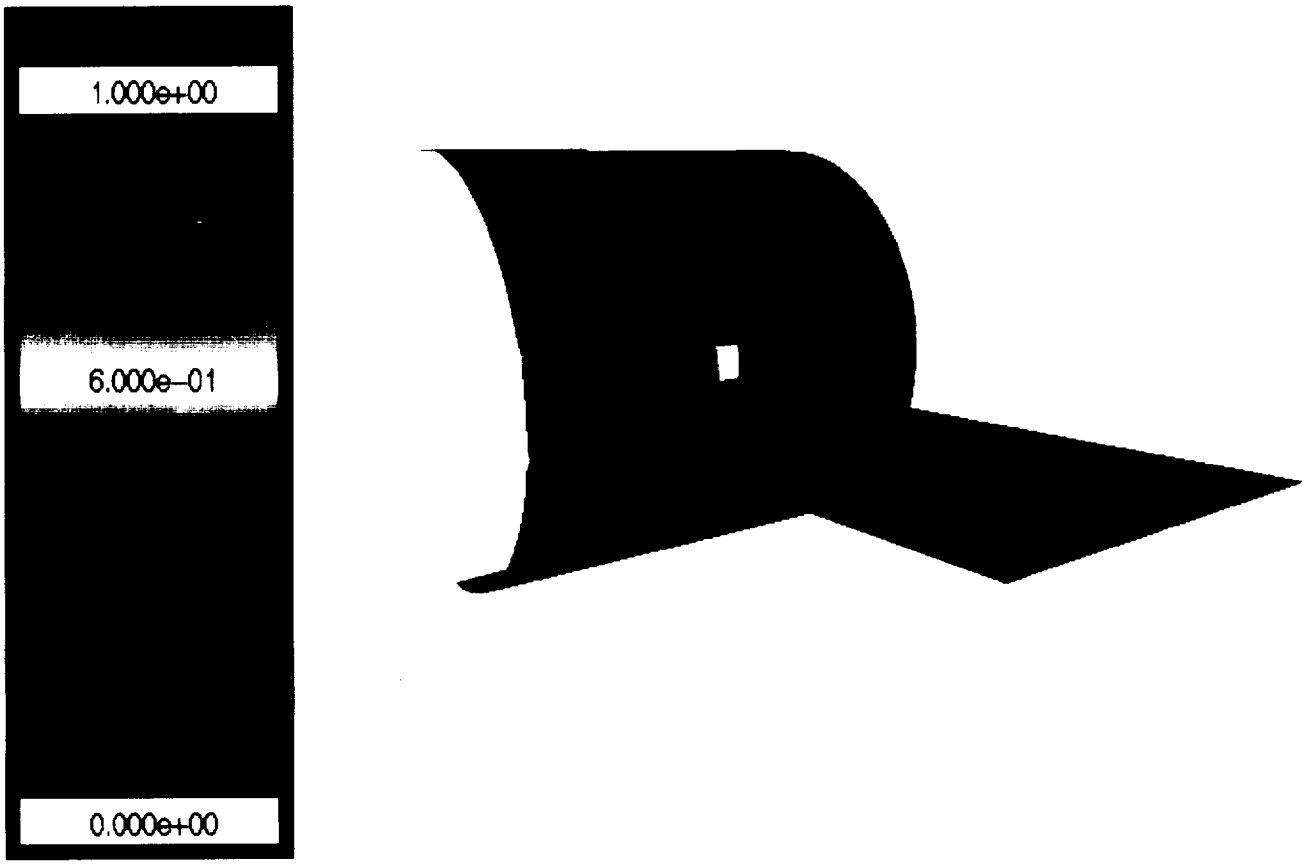

Plate 1. Benchmark problem featuring cylinder-plate junctures.
Lockheed PARL relative error estimation for 320 16-node ANS elements.

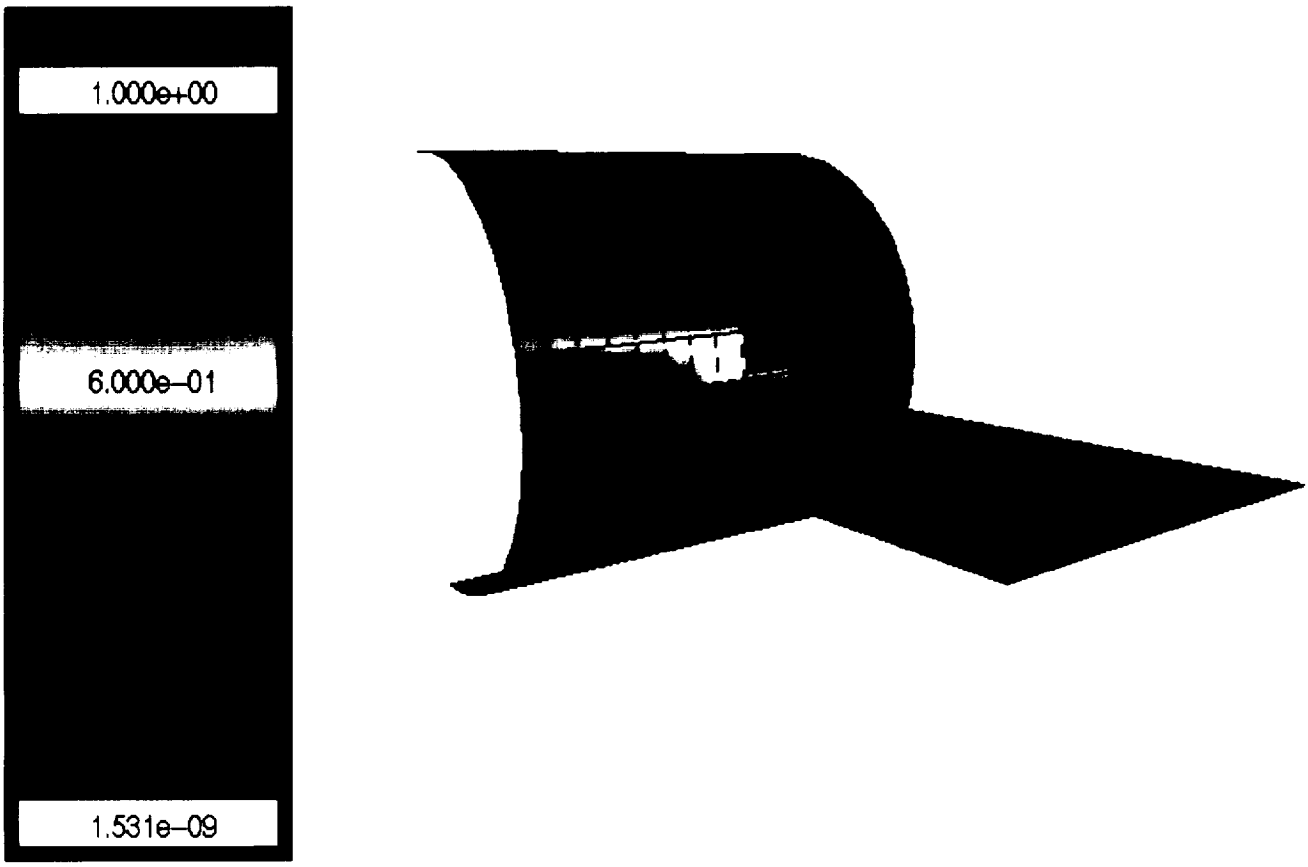

Plate 2. Benchmark problem featuring cylinder-plate junctures.
DM error indicator for 320 4-node ANS-EC elements.

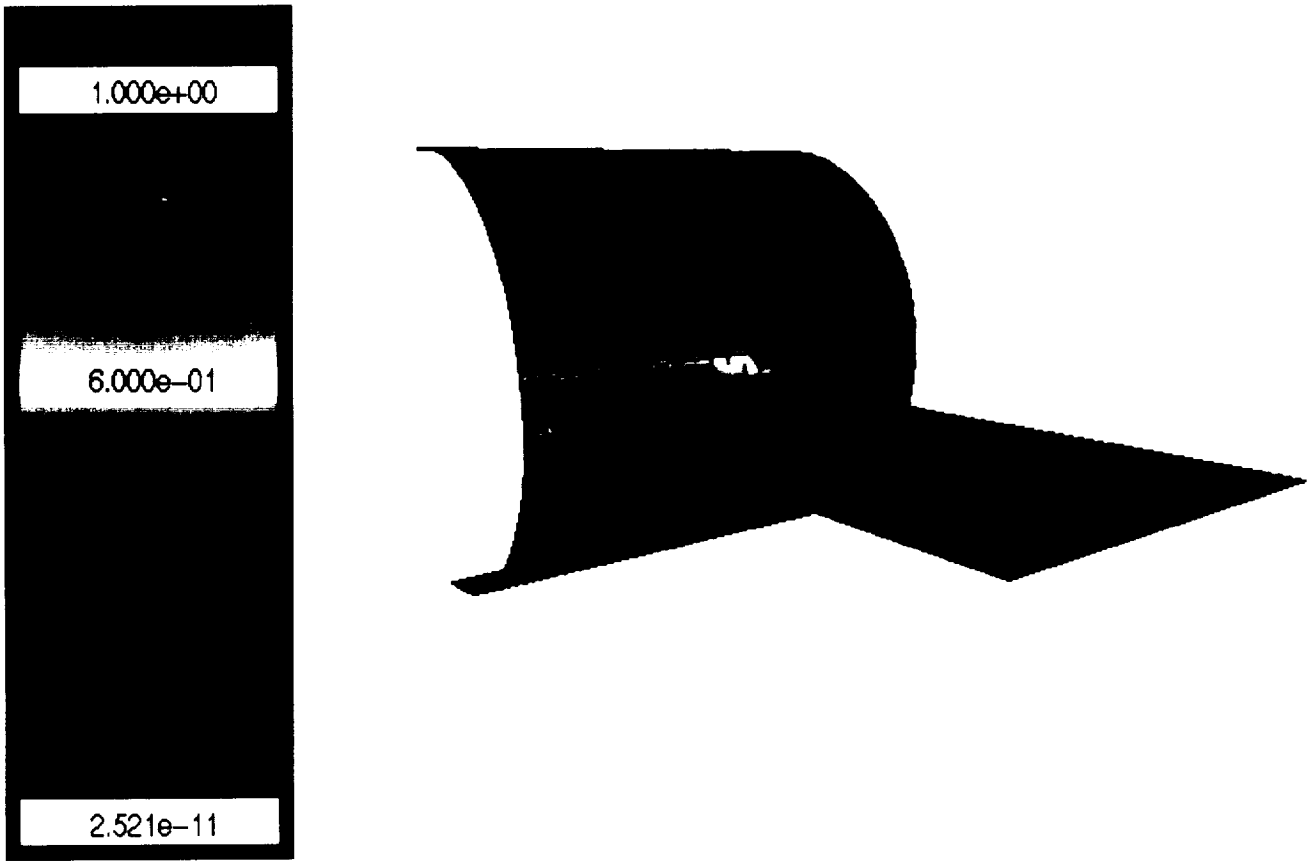

Plate 3. Benchmark problem featuring cylinder-plate junctures.
DM error indicator for 1056 4-node ANS-EC elements.

6. Summary

We have developed an element-level, element-independent error indicator known herein as the DM error indicator. This new error indicator is founded upon ideas stemming from two previous error indicators based on parameterized variational principles and one indicator based on an element-independent formulation. The element-independence of the new indicator is an important development because standard finite elements can now be used to predict error at the element-level. Use of standard finite elements is an important attribute for implementing this error indicator in production-level codes.

Since the error indicator is element-level, we can compute mesh discretization error, element-by-element, on parallel processing machines without imposed limitations from multiple domain decompositions. This is an important factor in solution of large-scale finite element problems.

We have defined two goals by which to conduct this research. To date, Goal 1 has been met and indications are that Goal 2 can likely be met.

Comparison of the DM error indicator to analytical solutions and to well-known error estimators reveals that this error indicator has potential for successfully returning true error estimates and driving adaptive mesh refinements.

7. Topics for Future Research

Two element-level, element-independent error indicators have been developed for use in various classes of problems. In addition, two adaptive mesh refinement techniques have been developed and used successfully. The logical completion of the current research is to improve both the DM error estimation and adaptive mesh refinement techniques. Completion of the error estimation and adaptive mesh refinement research requires realization of the following goals:

1. Quantitative evaluation of the current DM error indicator.
2. Parallel adaptive mesh refinement.
3. Application of the DM error indicator and parallel analysis procedures to more realistic aircraft shell structures.

7.1. Quantitative Evaluation of the DM Error Indicator

Numerical experiments have shown that the DM error indicator returns reasonable results for assessing the location of error in finite element models due to dominating modes. The next step will be to assess the quality of the error solution in terms of quantifying actual errors. For membrane-dominated problems the DM error indicator tends to underestimate actual error. The DM indicator has yet to be tested extensively for problems dominated by shear and bending.

In order to test the DM indicator's potential for realistic error estimation, a group of test problems featuring membrane bending, membrane shear, plate bending, plate shear and twisting will be analyzed. An initial assessment of the contribution to element strain energy error by each of (or combinations of) these modes can be made by considering a breakdown of shell element strain energies into three basic constitutive parts: membrane, bending and transverse shear:

$$U = U_m + U_b + U_s \tag{7.1.1}$$

where the subscripts m, b and s denote the membrane, bending and shear components, respectively. Computationally, this is readily accomplished for flat triangles and unwarped four node element by reformulating the element stiffness as

$$\mathbf{K}^e = \mathbf{K}^e_m + \mathbf{K}^e_b + \mathbf{K}^e_s \tag{7.1.2}$$

and computing the strain energy components as

$$U = \tfrac{1}{2}\left((\mathbf{v}^e)^T\mathbf{K}^e_m\mathbf{v}^e + (\mathbf{v}^e)^T\mathbf{K}^e_b\mathbf{v}^e + (\mathbf{v}^e)^T\mathbf{K}^e_s\mathbf{v}^e\right). \tag{7.1.3}$$

The various stiffness matrices, and hence the various strain energy components, may be obtained by adjusting the element constitutive model as desired for each component and recomputing the strain energy. Hence, by observing each of the strain energy components U_m, U_b and U_s, we can acquire general knowledge about the behavior of the element and the source of strain energy error. It is likely, for example, that an improved quantitative

error estimate can be obtained by setting the shear error energy to zero in the case of thin shells. The decomposition (7.1.3) applies to planar shell elements in which the various components are uncoupled. More rigorous analysis would be necessary for warped shell elements in which the components are coupled. Following this basic strain energy analysis procedure, detailed mode-by-mode analysis will be performed.

7.2. Parallel Implementation of Adaptive Mesh Refinement

Parallel implementation of adaptive mesh refinement can be used to augment parallel solution techniques. Our interest in parallel error estimation is now extended to the parallel refinement of meshes. Typically, in parallel analysis, a structural model is decomposed into a number of substructures. This technique is a special case of the so-called domain decomposition (DD) method. Fig. xx shows a structure decomposed into substructures numbered I-VII.

In parallel computation, each of the substructures would be assembled and solved on an individual processor. (The total solution might then be solved iteratively upon coupling the substructure solutions.) Element-level errors for the elements within a given substructure would also be computed on the respective substructure processor. As previously noted, the fact that all of the indicators developed here are element-level makes such a computation easily parallelizable.

To augment the parallel solution technique with mesh adaptation, we will see that *r*- and *h*-adaptation schemes have severe shortcomings and that a *rezoning* technique would be more appropriate. Prior to discussion of the new technique, we briefly examine the problems associated with those currently implemented.

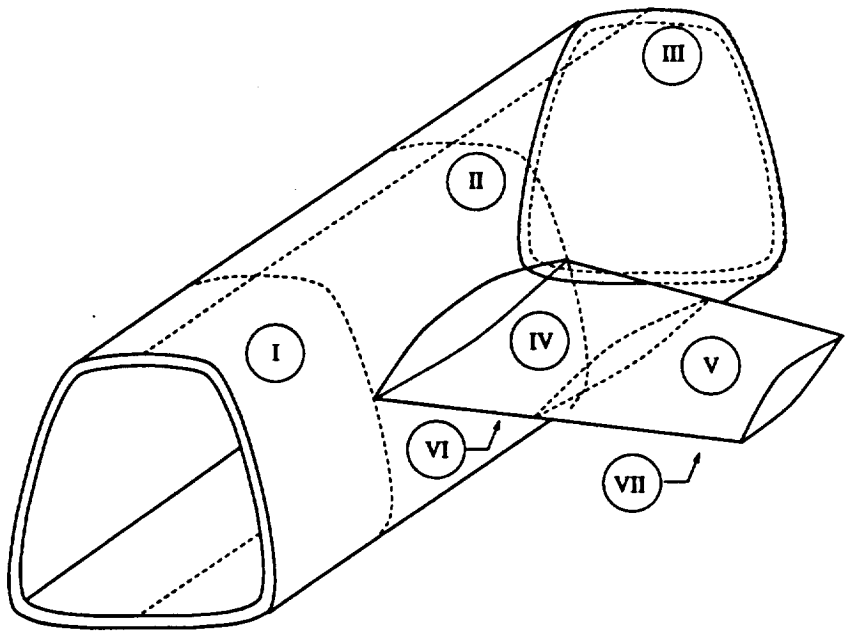

Fig. xx Shell structure model decomposed into seven subdomain substructures.

7.2.1. Limitations of the r- and h-adaptation techniques

We have shown the r- and h-adaptive refinement techniques to be effective methods for refining complete meshes and meshes composed of simple elements. However, both the r- and h-adaptive methods possess some shortcomings for mesh refinement.

The r-adaptive mesh refinement technique requires relocation of nodes throughout the mesh and along external and juncture boundaries. Nodes are effectively dragged to new locations by error-proportionate forces from surrounding elements. In domain decomposition, juncture boundaries are often curves along which a mesh is partitioned – recall the example showing possible decomposition of a structural model in Fig. xx. To retain mesh definition and displacement compatibility (barring the use of Lagrange multipliers or interface elements), the juncture between sections II and IV would be a curve along which nodes would travel if r-adaptation were being performed. Obviously, node relocation along the juncture would require repeated communication *across* the boundary which would violate the decomposition and incur significant processor communication overhead.

The h-adaptive mesh refinement technique is primarily limited to triangular elements. While some finite element codes employ this technique for other types of elements,[41] it is only done at the expense of creating elements with poor aspect or by sophisticated interelement constraints. Element density via h-adaptation is also limited by the size of the elements being split. In other words, even in areas of high error gradients, progressive refinements will only occur at a algebraic rate of $\frac{h}{2}$ where h is indicative of the element size. Another difficulty with parallel h-adaptation is that the extensive data structure changes may impact load balancing unless the substructure are reconstructed periodically, which can be very expensive. While h-adaptation is not in direct conflict with DD analysis, its limitations are significant enough to consider another technique.

7.2.2. The z-Adaptation Technique

Based on the limitations shown for r- and h-adaptive refinement techniques, it is proposed to replace them with a substructure remeshing scheme known for the present as z-adaptive mesh refinement. We define z-adaptation as "the total remeshing of a structure or substructure based on a given error distribution." A survey of common z-refinement schemes is given by Frykestig.[42] Of the many schemes described, advancing front methods appear to be preferable for refinement of general surfaces. Frykestig has shown advancing front methods work well with non-uniform rational B-spline surfaces (NURBS) [31]. These methods do not share many of the problems associated with other common z-refinement schemes (e.g., triangle degeneracies due to numerical round-off). A parallel implementation of rezoning may be performed by starting wavefront generation from each substructure boundary and progressing "inwards" in each.

7.3. Analysis of Aerospace Shell Structures

Following the evaluation and subsequent improvements to the DM error indicator, analyses of realistic aircraft-related shell structures will be performed. It is proposed that

general surface three dimensional test problems (perhaps derived from the CPJ benchmark problem) be analyzed and compared to analytical solutions or refined solution from an acceptable source.

Acknowledgements

This work has been supported by NASA Langley Research Center under Grant NAS1-756, monitored by Dr. J. Housner. We thank Bryan Hurlbut, Ishak Levit and Gary Stanley of the Structures Laboratory at Lockheed PARL for assistance in providing comparison solutions for the CPJ problem.

References

1. Fraeijs de Veubeke, B. M., "Upper and Lower Bounds in Matrix Structural Analysis," in *AGARDograph 72*, Pergamon Press, 1964.
2. Fraeijs de Veubeke, B. M., "Displacement and Equilibrium Models in the Finite Element Method," Chapter 9 of *Stress Analysis*, ed. by O. C. Zienkiewicz and G. Hollister, Wiley, New York, 1965.
3. Geradin, M., (ed.), *B. M. Fraeijs de Veubeke's Memorial Volume of Selected Papers*, Sithoff & Noordhoff Pubs., Alphen and den Rijn, The Netherlands, 1980.
4. Babuška, I., "The Selfadaptive Approach in the Finite Element Method." in *The Mathematics of Finite Elements and Applications II* MAFELAP 75, ed. by J. R. Whiteman, Academic Press, London, 1975, pp. 125–142.
5. Sewell, G., "An Adaptive Computer Program for the Solution of Div$(P(X,Y)$Grad$U) = F(X,Y,U)$ on a Polynomial Region," in *The Mathematics of Finite Elements and Applications II* MAFELAP 75, ed. by J. R. Whiteman, Academic Press, London, 1975, pp. 543–554.
6. Zienkiewicz, O. C. and Zhu, J. Z., "A Simple Error Estimator and Adaptive Procedure for Practical Engineering Analysis," *International Journal for Numerical Methods in Engineering*, **24**, 1987, pp. 337–357.
7. Zienkiewicz, O. C. and Zhu, J. Z., "The Superconvergent Patch Recovery and *A Posteriori* Error Estimates, Part 2: Error Estimates and Adaptivity," *International Journal for Numerical Methods in Engineering*, **33**, 1992, pp. 1365–1382.
8. Babuška, I., "The p and h-p Versions of the Finite Element Method. The State of the Art," *Inst. for Physical Sciences and Technology Note BN-1156*, Univ. of Maryland, 1986.
9. Zienkiewicz, O. C., Kelly, D. W., Gago, J. P. and Babuška, I., "Hierarchical Finite Element Approaches, Error Estimates and Adaptive Refinement," in *The Mathematics of Finite Elements and Applications IV (MAFELAP VI)*, Brunel University. ed. by J.R. Whiteman, Academic Press, New York, 1981.
10. Zienkiewicz, O. C. and Craig, A., "A-posteriori Error Estimates and Adaptive Mesh Refinement in the Finite Element Method Concepts," Chapter 5 in *The Mathematical Basis of Finite Element Methods*, ed. by D. Griffiths, Clarendon Press, Oxford, 1984.
11. Zienkiewicz, O. C. and Craig, A., "Adaptive Refinement, Error Estimates, Multigrid Solution and Hierarchic Finite Element Method Concepts, Chapter 2 in *Accuracy Estimates and Adaptive Refinements in Finite Element Computations*, ed. by I. Babuška *et.al.*, John Wiley and Sons, Chichester, 1986.
12. Babuška, I., Zienkiewicz, O. C., Gago, J. and Oliveira, E. L., *Accuracy Estimates and Adaptive Refinements in Finite Element Computations*, Wiley, Chichester, 1981.
13. Szabó, B. A. and Babuška, I., *Finite Element Analysis*, Wiley-Interscience, New York, 1991.

14. Felippa, C. A. and Militello, C., "Developments in Variational Methods for High Performance Plate and Shell Elements," in *Analytical and Computational Models for Shells*, CED Vol. 3, ed. by A. K. Noor, T. Belytschko and J. C. Simo, ASME, New York, 1989, pp. 191–216.

15. Felippa, C. A. and Militello, C., "Variational Formulation of High Performance Finite Elements: Parametrized Variational Principles," *Computers & Structures*, **36**, 1990, pp. 1–11.

16. Felippa, C. A., "Parametrized Multifield Variational Principles in Elasticity: I. Mixed Functionals," *Communications in Applied Numerical Methods*, **5**, 1989, pp. 69–78.

17. Felippa, C. A., "Parametrized Multifield Variational Principles in Elasticity: II. Hybrid Functionals and the Free Formulation," *Communications in Applied Numerical Methods*, **5**, pp. 79–88.

18. Felippa, C. A., "The Extended Free Formulation of Finite Elements in Linear Elasticity," *Journal of Applied Mechanics*, **56**, 1989, pp. 609–616.

19. Militello, C. and Felippa, C. A., "A Variational Justification of the Assumed Natural Strain Formulation of Finite Elements: I. Variational Principles," *Computers & Structures*, **34**, 1990, pp. 431–438

20. Militello, C. and Felippa, C. A., "A Variational Justification of the Assumed Natural Strain Formulation of Finite Elements: II.The Four-Node C^0 Plate Element," *Computers & Structures*, **34**, 1990, pp. 439–444

21. Militello, C., *Application of Parametrized Variational Principles to the Finite Element Method*, Ph. D. Dissertation, Department of Aerospace Engineering Sciences, University of Colorado, Boulder, CO, 1991.

22. Felippa, C. A. and Militello, C., "Membrane Elements with Corner Drilling Freedoms: II: The ANDES element," *Finite Elements in Analysis and Design*, **12**, 1992, pp. 189–201

23. Park, K. C., and G. M. Stanley, "A Curved C^0 Shell Element Based on Assumed Natural-Coordinate Strains," *Journal of Applied Mechanics*, **53**, 1976, pp. 278–290.

24. Bergan, P. G., and Nygård, M. K., "Finite Elements with Increased Freedom in Choosing Shape Functions," *International Journal of Numerical Methods in Engineering*, **20**, 1984, pp. 643–664.

25. Beltrán, F. J., *Estimadores de error basados en principios variacionales multicampo para cálculos por elementos finitos*, Tesis Doctoral, Universidad Politécnica de Madrid, 1990.

26. Beltrán, F. J. and Alarcón, E., "Estimadores de Error Basados en Principios Variacionales Multicampo," in *Memorias I Congreso de Métodos Numéricos de Ingeniería*, ed. by G. Winter and M. Galante, Sociedad Española de Métodos Numéricos en Ingeniería, Barcelona, Spain, 1990, pp. 683–689.

27. Melosh, R. J. and Marcal, P. V., "An Energy Basis for Mesh Refinement of Structural Continua," *International Journal for Numerical Methods in Engineering*, **11**, 1977, pp. 1083–1091.

28. Militello, C. and Felippa, C. A., "r-Adaptive Methods Based on Element-Level Error Indicators for Parallel Analysis of Plates and Shells," *Proc. 33rd AIAA/ASME/AHS/ASC SDM Conference*, Dallas, TX, April 1992

29. Keating, S. C., Felippa, and C. A., Militello , C., "Implementation of a Mesh Adaptive Scheme Based on an Element-Level Error Indicator," *Proc. 34th AIAA/ASME/AHS/ASC SDM Conference*, LaJolla, CA, April 1993

30. Alvin, K., de la Fuente, H. M., Haugen, B. and Felippa, C. A., "Membrane Elements with Corner Drilling Freedoms: I: The EFF Element," *Finite Elements in Analysis and Design*, **12**, 1992, pp. 163–187

31. Haugen, B., *Buckling and Stability Problems for Thin Shell Structures using High Performance Finite Elements* , Ph. D. Dissertation, University of Colorado at Boulder, 1994.

32. Choi, B. K., *Surface Modeling for CAD/CAM* , Elsevier, Amsterdam, 1991.

33. Farin, G., *Curves and Surfaces for Computer Aided Geometric Design (A Practical Guide)*, 2nd Edition, Academic Press, Inc., 1990.

34. Nowacki, H., and Reese, D., "Design and fairing of ship surfaces," *Surfaces in Computer Aided Graphic Design*, Barnhill, R. and Boehm, W., (editors), North-holland, Amsterdam, 1983.

35. Walter, H., *Numerical representation of surfaces using an optimum principle* , (in German), Ph. D. Thesis, Munich, 1971.

36. Hagen, H. and Schulze, G., "Automatic smoothing with geometric surface patches," *Computer Aided Geometric Design*, Vol. 4, 1987.

37. Farin, G. and Hagen, H., "Optimal Twist Estimation," , *Surface Design*, Hagen, H. (editor), SIAM Philadelphia, 1992.

38. Oden, J. T., Demkowicz, W., Rachowicz, W. and Westermann, T. A., "Toward a universal *h-p* adaptive finite element strategy, Part 2, *A posteriori* error estimation," *Comp. Methods Appl. Mech. Eng.*, **77**, 1989, pp. 113–180

39. Hurlbut, B., Levit, I. and Stanley, G. M., Private communication, January 1993.

40. Jensen, D.D., *Equilibrium Constrained Assumed Natural Coordinate Strain Finite Elements for Shell Analysis*, Ph. D. Dissertation, University of Colorado at Boulder, 1992.